

AMERICAN UNIVERSITY OF BEIRUT

STEEL SHEAR ENDPLATE CONNECTIONS IN FIRE:
RESISTANCE AND DEMAND USING FINITE ELEMENT
AND MECHANISTIC MODELING

by
SARAH AKRAM SLEIMAN

A thesis
submitted in partial fulfillment of the requirements
for the degree of Master of Engineering
to the Department of Civil and Environmental Engineering
of the Faculty of Engineering
at the American University of Beirut

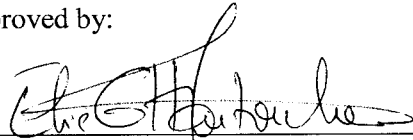
Beirut, Lebanon
July 2015

AMERICAN UNIVERSITY OF BEIRUT

STEEL SHEAR ENDPLATE CONNECTIONS IN FIRE:
RESISTANCE AND DEMAND USING FINITE ELEMENT
AND MECHANISTIC MODELING

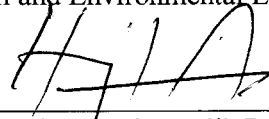
by
SARAH AKRAM SLEIMAN

Approved by:



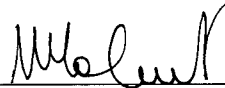
Dr. Elie Hantouche, Assistant Professor
Civil and Environmental Engineering

Advisor



Dr. Muhammad Harajli, Professor
Civil and Environmental Engineering

Member of Committee



Dr. Mounir Mabsout, Professor
Civil and Environmental Engineering

Member of Committee

Date of thesis defense: [July 1, 2015]

AMERICAN UNIVERSITY OF BEIRUT

THESIS, DISSERTATION, PROJECT RELEASE FORM

Student Name: _____
Sleiman Sarah Akram

Master's Thesis Master's Project Doctoral Dissertation

I authorize the American University of Beirut to: (a) reproduce hard or electronic copies of my thesis, dissertation, or project; (b) include such copies in the archives and digital repositories of the University; and (c) make freely available such copies to third parties for research or educational purposes.

I authorize the American University of Beirut, **three years after the date of submitting my thesis, dissertation, or project**, to: (a) reproduce hard or electronic copies of it; (b) include such copies in the archives and digital repositories of the University; and (c) make freely available such copies to third parties for research or educational purposes.

Signature

Date

ACKNOWLEDGMENTS

First, I would like to express my sincere gratitude to my advisor Dr. Elie Hantouche for his full support, help and encouragement.

I would like to thank the American University of Beirut for giving me this opportunity as a student here.

My recognition and gratitude are addressed to my committee Dr. Muhammad Harajli and Dr. Mounir Mabsout.

Finally, I would also like to thank my colleagues, friends, and family for being there for me.

AN ABSTRACT OF THE THESIS OF

Sarah Akram Sleiman for Master of Engineering
Major: Civil Engineering

Title: Steel Shear Endplate Connections in Fire: Resistance and Demand using Finite Element and Mechanistic Modeling

Shear endplate connections are one of the common simple beam-end framing connections used in steel structures, but their strength and deformation capacities in fire are not adequately understood. Very limited experimental studies have been conducted on full scale shear endplate beam-column assemblies. In this study, a series of finite element (FE) simulations and mechanistic modeling of steel shear endplate beam-column connections is developed to predict their behavior during fire. First, FE models are developed and validated against experimental results at ambient and elevated temperature. Second, a parametric study is conducted to investigate some major parameters that impact the behavior of shear endplate connections assemblies during a fire. This includes beam length, load ratio, initial cooling temperature, endplate thickness, endplate location, and beam depth. A comparison is also made between the performances of shear endplate, double angle and shear tab connections at elevated temperatures. The results show that although the axial load demand on the shear endplate connection is larger, the tension bolts in the shear endplate connection are more vulnerable to failure when compared to shear tab and double angle connections. Based on the FE and experimental results, a mechanistic model is proposed for the connection. The characteristics of the proposed model such as stiffness, tension, and compression are determined based on each component of the connection. The proposed model is capable of predicting the behavior of the connection and beam for different geometric properties and under varied loading conditions and elevated temperatures. This study provides guidelines for engineers to quantify and predict the fire induced thermal loads and their implications on fire design of steel framed buildings.

CONTENTS

ACKNOWLEDGEMENTS.....	v
ABSTRACT.....	vi
LIST OF ILLUSTRATIONS.....	x
LIST OF TABLES.....	xii
LIST OF ABBREVIATIONS.....	xiii
Chapter	
I. INTRODUCTION AND LITERATURE REVIEW.....	1
A. Introduction	1
B. Literature Review	1
C. Thesis Objective and Organization.....	3
II. ISOLATED SHEAR ENDPLATE CONNECTION: PREDICTION OF STRENGTH CAPACITY.....	5
A. Development of the FE Model	5
B. Geometry of the Connection Components	6
1. Geometry of the Connection Components.....	6
2. Material Properties	7
3. Model Discretization	8
4. Analysis Procedure	8
5. FE vs. Experimental Predictions	9

III. SHEAR ENDPLATE CONNECTION ASSEMBLY: EVALUATIONS OF DEMAND	12
A. Description of the Connection Assembly Model	14
B. Effect of Key Parameters and Connection Details	15
1. Load Ratio.....	15
2. Beam Length	18
3. Initial Cooling Temperature.....	21
4. Shear Endplate Location.....	23
5. Shear Endplate Thickness	24
6. Beam Depth.....	26
IV. COMPARISON OF SHEAR ENDPLATE, SHEAR TAB AND DOUBLE ANGLE CONNECTION ASSEMBLIES	27
V. MECHANISTIC MODELING FOR PREDICTING THE THERMAL-INDUCED AXIAL FORCES OF SHEAR ENDPLATE CONNECTIONS IN FIRE	32
A. Description of the Behavior	34
1. Proposed Model I	34
2. Proposed Model II.....	34
B. Elastic and Plastic Stiffness of the Connection.....	35
C. Formulation of the Response for Proposed Model I.....	38
1. Mechanism in (s1).....	38
2. Mechanism in (s2).....	39
3. Mechanism in (s3).....	44
4. Mechanism in (s4).....	47
D. Formulation of the response for proposed model II.....	49
1. Mechanism in (s1).....	50
2. Mechanism in (s2).....	51
3. Mechanism in (s3).....	51
4. Mechanism in (s4).....	52
3. Mechanism in (s5).....	52

4. Mechanism in (s6).....	53
E. Mechanistic Model vs. FE Results.....	53
VI. CONCLUSIONS	57
BIBLIOGRAPHY	61

ILLUSTRATIONS

Figure	Page
1. Connection details in the FE model.....	5
2. Strength retention factors for structural steel, structural bolts, and weld material at elevated temperatures.....	7
3. Force-rotation behavior of shear endplate connections at ambient and elevated temperature; FE results compared with experimental results.....	9
4. (a) Deformed shape obtained from the FE simulation at 20° C, (b) Experiment-deformed shape at 20° C, (c) Deformed shape obtained from the FE simulation at 550° C, (d) Experiment-deformed shape at 550° C.....	10
5. Layout of connection assemblies used in parametric study. (a) Shear endplate connection, (b) Double angle connection, (c) Shear tab connection.....	13
6. (a) Axial force in the shear endplate during heating and cooling for a varying load ratio, (b) Top bolt force comparison during heating for a varying load ratio.....	16
7. (a) Beam rotation for varying load ratios (W16), (b) Definition of beam rotation.....	17
8. Endplate uplift for varying load ratios (W16).....	18
9. (a) Axial force in the shear endplate for varying beam lengths (W16), (b) Top bolt force comparison for varying beam lengths (W16)....	19
10. (a) Beam rotation for varying beam lengths (W16), (b) Endplate uplift for varying beam lengths (W16).....	20
11. (a) Axial force in the shear endplate for varying initial cooling temperatures (W16), (b) Top bolt force comparison for varying initial cooling temperatures (W16).....	22
12. Axial force in the shear endplate for varying endplate locations (W16).....	23
13. Axial force in the shear endplate for a varying endplate thickness (W16).....	24
14. (a) Beam rotation comparison for different endplate thicknesses (W16) (b) Endplate uplift for a varying endplate thickness (W16).....	25

15.	Axial force in the shear endplate for a varying beam depth.....	26
16.	(a) Axial force in the shear tab, double angle, and shear endplate connections, (b) connection rotation for the shear tab, double angle, and shear endplate connections.....	30
17.	(a) Comparison of shear bolt force in the shear tab and double angle, (b) Comparison of the top tension bolt force for the double angle and the shear endplate connections.....	31
18.	Typical variation of the axial force with temperature for a shear endplate connection,(a) type I, (b) type II.....	33
19.	(a) Model of beam, connection and column as used in the mechanistic model, (b) von Mises stress contour in the beam at the beginning of the heating stage (<i>sI</i>).....	35
20.	The reduction in the area of the beam web at the current step (<i>i</i>) as a function of the axial force at the previous step (<i>i-1</i>).....	41
21.	Contact between the lower beam flange and the column.....	43
22.	(a) The increase in the flange contact area contributing to the axial as a function of the axial force at the previous step, (b) increased deflection in the beam after lower beam flange buckling, (c) tributary contact area of the beam web	45
23.	Flowchart of the incremental stiffness shear endplate model.....	54
24.	Comparison of the FE results with the proposed model for different cases: (a) case 14, (b) case 32, (c) case 17.....	55
25.	Comparison of the FE results with the proposed model for different cases: (a) case 16, (b) case 31, (c) case 30.....	56

TABLES

Table		Page
1.	Comparison of experimental results and FE results.....	11
2.	Failure modes and temperatures for the shear endplate, double angle, and shear tab connections.....	29
3.	Buckling and contact parameters for different load ratios, beam lengths, and endplate thickness.....	42

ABBREVIATIONS

a_1 : slope for linear relation between the reduction beam web area and the axial force at the previous step $P_{(i-1)}$

a_2 : slope for linear relation between the flange contact area and the axial force at the previous step $P_{(i-1)}$

A_b : the cross sectional area of the beam

$A_{bc(i)}$: total beam section area contributing to the axial force at the current step (temperature $T_{(i)}$)

$A_{bc(max)}$: beam section area contributing to the axial force at T_{Pmax}

$A_{bfc(i)}$: contact flange area contributing to the axial force at the current step (temperature $T_{(i)}$)

$A_{bfc(i-1)}$: flange contact area at the previous step

b_w : area of the beam web

A_{bwr} : reduced beam web area at the end of (s_2) (at the onset of contact)

$A_{bwr(i)}$: reduced beam web area at the current step

$A_{bwr(i-1)}$: beam web area at the previous step

A_{ct} : area of the beam section working in catenary

a_p : size of the fillet weld

b_1 : y-intercept for linear relation between the reduction beam web area and the axial force at the previous step $P_{(i-1)}$

b_2 : y-intercept for linear relation between the flange contact area and the axial force at the previous step $P_{(i-1)}$

$B_{cr(i)}$: critical bolt force at a the current step (temperature $T_{(i)}$)

b_{eff-c} : effective buckling width of the column web

b_{effcw} : assumed effective width of the column web

$B_{f(i)}$: the bolt force at any given temperature $T_{(i)}$

d_b : beam depth

d_c : depth of the column

d_{cw} : depth of the column web between fillets

d_p : depth of the plate

E : modulus of elasticity

$E_{b(i)}$: modulus of elasticity of the beam at current step (temperature $T_{(i)}$)

$E_{Tb(i)}$: tangent modulus of elasticity of beam at a certain temperature $T_{(i)}$ (current step)

$E_{c(i)}$: modulus of elasticity of the column at current step (temperature $T_{(i)}$)

$E_{Tc(i)}$: tangent modulus of elasticity of the column at a certain temperature $T_{(i)}$ (current step)

F : matrix of external applied forces at the nodes

$f_{yb(i)}$: yield stress in the beam

$f_{yc(i)}$: column yield strength at at current step (temperature $T_{(i)}$)

I_b : moment of inertia of the beam

k : stiffness of the spring element

K_b : beam element stiffness matrix

K : global matrix for the system

$K_{(i)}$: stiffness of the spring element at current step (temperature $T_{(i)}$)

K_s : spring element stiffness matrix

l_l : distance from the edge of the endplate to the external side of the lower flange of the beam

L_b : length of the beam

M : applied moment on the beam

n_{tb} : number of tension bolts in the connection

P : internal axial force in the beam

$P_{500^\circ\text{C}}$: thermal axial force when the temperature reaches 500°C

$P_{bfc(i)}$: contribution of the lower flange of the beam to the total axial compressive force at the current step (temperature $T_{(i)}$)

$P_{bfy(i)}$: lower beam flange yielding axial force at a certain temperature $T_{(i)}$ (current step)

$P_{bwy(i)}$: beam web yielding axial force at a certain temperature $T_{(i)}$ (current step)

P_{crbw} : axial force at the end of (sI) , actual beam web buckling load

$P_{crbw(i)}$: beam web critical buckling load at at current step (temperature $T_{(i)}$)

$P_{crcw(i)}$: force that causes buckling in the column at at current step (temperature $T_{(i)}$)

$P_{(i)}$: the internal axial force at current step (temperature $T_{(i)}$)

$P_{(i)}$: modification factor to reduce the moment of inertia of the beam at the current step (temperature $T_{(i)}$)

$P_{(i-1)}$: axial force at the previous step

P_{max} : maximum axial force (at T_{Pmax})

$q_{(i)}$: ratio of the plastic strain to the elastic strain at a certain temperature T_i (current step)

r_c : root radius of the column

$s1$: segment 1

$s2$: segment 2

$s3$: segment 3

$s4$: segment 4

$s5$: segment 5

$s6$: segment 6

t_{bf} : thickness of the beam flange

t_{cf} : thickness of the column flange

t_{cw} : column web thickness

t_e : shear endplate thickness

$T_{(i)}$: temperature at the current step

$T_{(i-1)}$: temperature at the previous step

T_{Pmax} : lower beam flange plastic buckling temperature

w : applied load on the beam (distributed load)

α : coefficient of thermal expansion

$\alpha_{(i)}$: coefficient of thermal expansion at current step (temperature $T_{(i)}$)

Δ : vector of nodal displacements

ΔA_{bfc} : flange contact area increment

ΔA_{bwr} : beam web area increment

ΔP : axial force increment

ΔT : temperature increment

ΔT : temperature increment

θ_c : geometric angle of contact between the bottom beam flange and the column

$\theta_{(i)}$: beam end rotation at the current step (temperature $T_{(i)}$)

CHAPTER I

INTRODUCTION AND LITERATURE REVIEW

A. Introduction

Shear endplate connections, also known as flexible endplates are widely used to connect steel beams to columns or girders in multi-story buildings. These connections possess large rotational ductility, and are considered as pinned joints. According to the design guidelines at ambient temperature, only gravity loads are accounted for in the procedure. However, during a fire event, shear or pinned connections are subjected to large axial forces, rotational demands, and significant loss of strength and stiffness, as observed by Ramli-Sulong et al. [1]. Bailey et al. [2] stated that the lateral restraint provided against the thermal expansion of beams results in compressive forces in the heating phase of the fire. At the end of the heating phase, tensile forces start to develop. Furthermore, tension develops in the connections as the beams contract during the cooling phase of the fire. The large thermally induced forces and demands may result in failure of the connections during or after fire.

B. Literature Review

Many experimental and analytical studies were conducted in the past few years to understand the behavior of shear endplate connections at elevated temperature. Al-Jabri [3,4] and Al-Jabri et al. [5,6] conducted an experimental investigation to study the performance of composite shear endplate connections in fire. Also, a mechanistic model was developed by the same authors to predict the behavior of the connections at elevated temperature. However, these studies and models only apply for the case of

unobstructed rotation about the lower edge of the endplate, assuming no contact between the beam and column flange, and do not predict the thermally induced forces on the connection. In addition, Hu et al. [7,8] investigated the capacity strength of shear endplate connection in fire both experimentally and analytically. The governing failure mode encountered was plate rupture in the vicinity of the weld. Yu et al. [9] developed a mechanistic model for simulating the behavior of flexible endplates in fire.

Studies were also conducted on other types of shear connections such as shear tab, double angle, top and seat angle, and extended endplate connections. For instance, Wang et al. [10,11] developed a mechanistic model to predict the behavior of extended endplate bare-steel joints at elevated temperature. Hu and Engelhardt [8,12] conducted experiments and finite element (FE) simulations to study the behavior of shear tab connections at elevated temperature, and to characterize their stiffness, strength, deformation capacity, and failure modes. They also studied the impact of several parameters (load ratio, stiffness of the adjacent structure, short-slotted bolt holes, shear tab location, and bolt grade) on the connection response. In addition, Daryan and Yahyai [13] conducted experimental tests and FE simulations to study the behavior of bolted top and seat angle connections in fire. Kodur et al. [14] developed FE models to predict the behavior of typical beam–slab assemblies with different shear connection types (welded and bolted shear tab and double angle connections), exposed to different fire scenarios. In a recent work, Selamat and Garlock [15,16,17] studied the behavior of shear tab, single angle, and double angle shear connections in fire. The connections were tested as part of a subassembly. They showed that the different shear connection types have similar global behavior. The response was governed by beam local buckling near the connection. More recently, Hantouche et al. [18] studied the behavior of bolted

double angle connections in fire. FE models for double angle connections were developed in ABAQUS [19] and validated against experimental data from the literature at both ambient and elevated temperatures. Also, the impact of several parameters (load ratio, initial cooling temperature, double angle location, and gap distance) on the behavior of double angle connection assemblies during a fire was investigated. Despite the progress that was made in understanding the capacity of shear endplate connections at elevated temperature, large gaps still exist. For instance, limited research has been conducted to predict the thermal induced forces and deformations experienced on shear endplates in fire. Therefore, it is necessary to better understand the force and deformation demand on shear endplates in fire, and to predict and characterize their strength and deformation capacities at elevated temperatures.

C. Thesis Objective and Organization

This study aims at providing a thorough understanding of the performance of shear endplate connections in fire by developing FE and mechanistic models that predict their behavior in fire. First, FE models of isolated shear endplate connections at ambient and elevated temperatures are developed and validated against experimental results available in the literature. Second, FE models of the connection assembly are generated and used to conduct an extensive parametric study to identify the key parameters that affect the behavior of the connection. The results of the study are then used to develop a mechanistic model that predicts the thermal induced axial forces applied on the connection. Also, a comparison of the performance of the shear endplate, shear tab, and double angle connection in a fire is performed. Design

guidelines are provided to quantify the thermal-induced forces during the heating and cooling phases of a fire and their implications on fire design of steel framed buildings.

CHAPTER II

ISOLATED SHEAR ENDPLATE CONNECTION: PREDICTION OF STRENGTH CAPACITY

The FE model of the shear endplate connection is developed. The FE results of shear endplate connections are compared with those obtained in the experimental program at University of Sheffield [19].

A. Development of the FE Model

The FE model of the shear endplate connection is developed to reproduce the experimental results conducted at the University of Sheffield [20]. An overall view of the model is shown in Fig. 1. The FE model of the connection was developed in ABAQUS [19].

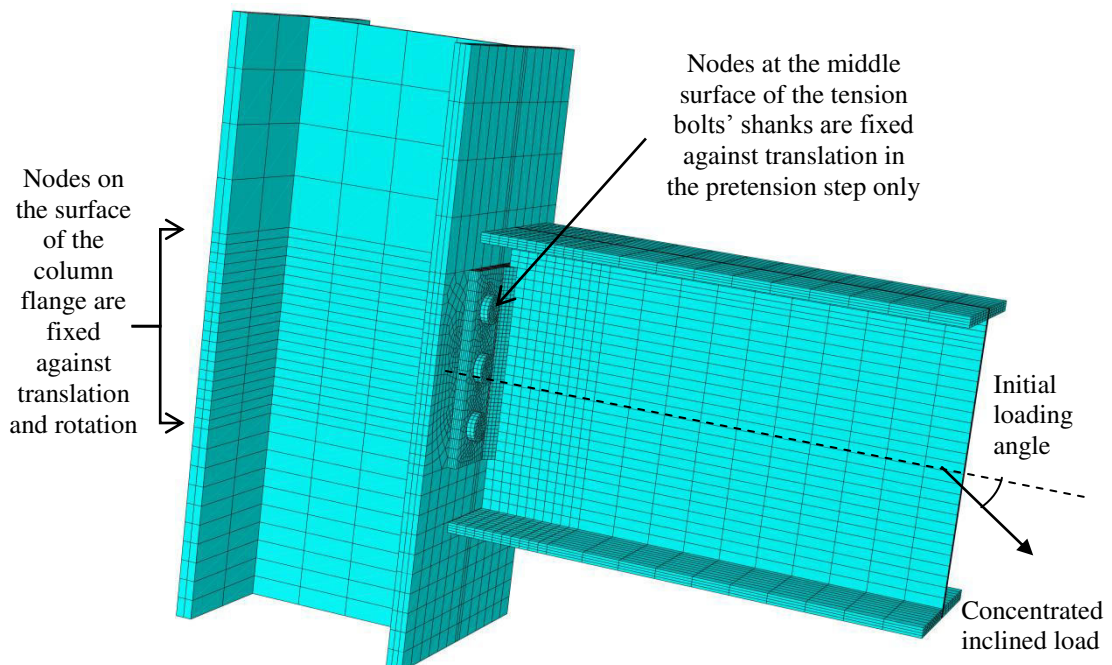


Fig. 1. Connection details in the FE model

B. Geometry of the Connection Components

The shear endplate connection used in the analysis consists of a PL 8×6×0.4 in. (PL 200×150×10 mm) bolted to the flange of a W10×60 (UC 254×89) column and welded to the web of a W12×26 (UB 305×40) beam cross-section. Details of the connection configuration can be found in [20].

1. Geometric and Force Boundary Conditions

The model is loaded in two steps. In the first step, a pretension force is applied to the bolts. The bolt pre-tensioning is modeled by applying a body force in the bolts equivalent to the minimum required pretension force specified in the AISC specifications [21]. In the second step, an inclined force is applied at the tip of the beam (Fig. 1), to produce combined shear and tension forces. The initial loading angle is 35° for the cases where the temperature is 20°C, 450°C, and 550°C, and 45° for the case where the temperature is 650°C. Throughout the load step, the loading angle varies and is described in the experimental program [20].

Boundary conditions are applied on the system throughout the analysis as shown in Fig. 1. During the pre-tension step, the bolts are restrained against any translation to ensure contact between the bolt head and nut, and base material. The endplate is also restrained from translation to ensure its contact with the tension bolts, the beam, and the column. During the loading step, all the boundary conditions are deactivated.

2. Material Properties

An idealized bilinear model is used for the steel materials. The ambient temperature mechanical properties used for the beam are: the yield stress $F_y = 52$ ksi (356 MPa), and the ultimate stress $F_u = 73$ ksi (502 MPa) which are in accordance with Hu et al. [7]. For the shear endplate, the material model specified in Hu et al.[7] with $F_y = 50$ ksi (350 MPa) and $F_u = 66$ ksi (455 MPa) is incorporated in the FE model. For the column, the ambient-temperature mechanical properties used are A572Gr50 (S355) as specified by the experimental program [20]. For the structural bolts, an elastic-perfectly plastic material model is used. The ambient-temperature mechanical properties incorporated in the FE model for the structural bolts are: $F_u = 135$ ksi (930 MPa) which are in accordance with Hu et al. [7].

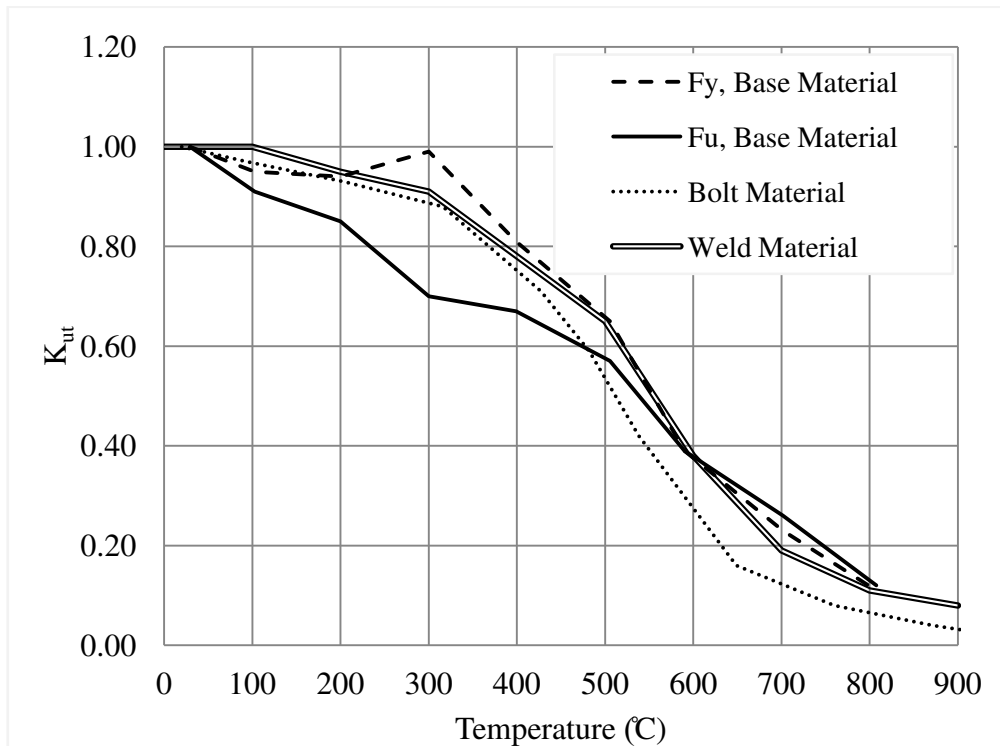


Fig. 2. Strength retention factors for structural steel, structural bolts, and weld material at elevated temperatures

At elevated temperature, retention factors proposed by Lee et al. [22] are used for the base material whereas the retention factors proposed by the AISC specifications [23] and Eurocode 3 [24] are used for the bolts and welds, respectively. Fig. 2 shows the retention factors for mechanical properties of structural bolt, weld, and steel materials incorporated in connection simulations.

3. Model Discretization

All the connection components are meshed with eight-node brick elements with reduced integration (C3D8-R). Fig. 1 shows the mesh configuration of the model. To improve the accuracy of predictions, a finer mesh is used around the connection region, where failure is likely to occur. Moreover, to account for stress concentration around the bolt-holes, a mapped meshing technique was used to discretize bolts and their surrounding areas.

The surface interactions between the bolt shank, shear endplate, and the column are modeled using finite sliding, with a friction coefficient of 0.25. The fillet welds are tied to adjacent parts by means of tie constraints applied at the contact surfaces.

4. Analysis Procedure

To predict the strength of the flexible endplate connection at elevated temperature, steady state analysis is conducted. After heating the structure up to the desired temperature (20°C, 450°C, 550°C, and 650°C), a concentrated inclined load is applied while keeping the temperature constant, until failure of the connection. Note that the post ultimate behavior of the structure is not predicted. The objective is

identifying the limit states in the connection at the specified temperatures under combined tension and shear loads.

5. FE vs. Experimental Predictions

The FE results are plotted against the experimental test results conducted at the University of Sheffield [20]. FE results show good agreement when compared with experimental results as far as strength, stiffness, and rotation, as shown in Fig. 3.

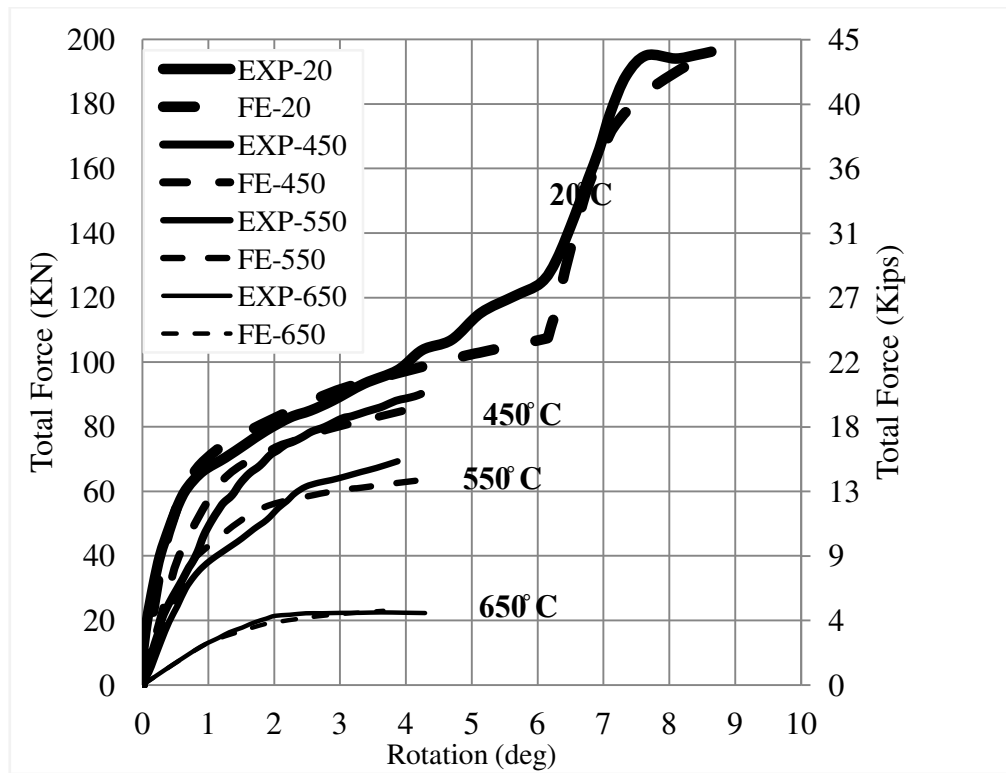


Fig. 3. Force-rotation behavior of shear endplate connections at ambient and elevated temperature; FE results compared with experimental results

The deformed shape and the failure mode of the shear endplate connection at ambient and elevated temperature are shown in Figs. 4(a), 4(b), 4(c), and 4(d). It can be seen from Figs. 3 and 4 that the FE simulation can predict closely the force-deformation response of the connection as well as the failure mode which is plate rupture at the toe of the weld.

The results of the capacity predictions and the comparison between the experimental and FE results are summarized in Table 1. The FE models predict the peak connection strength well.

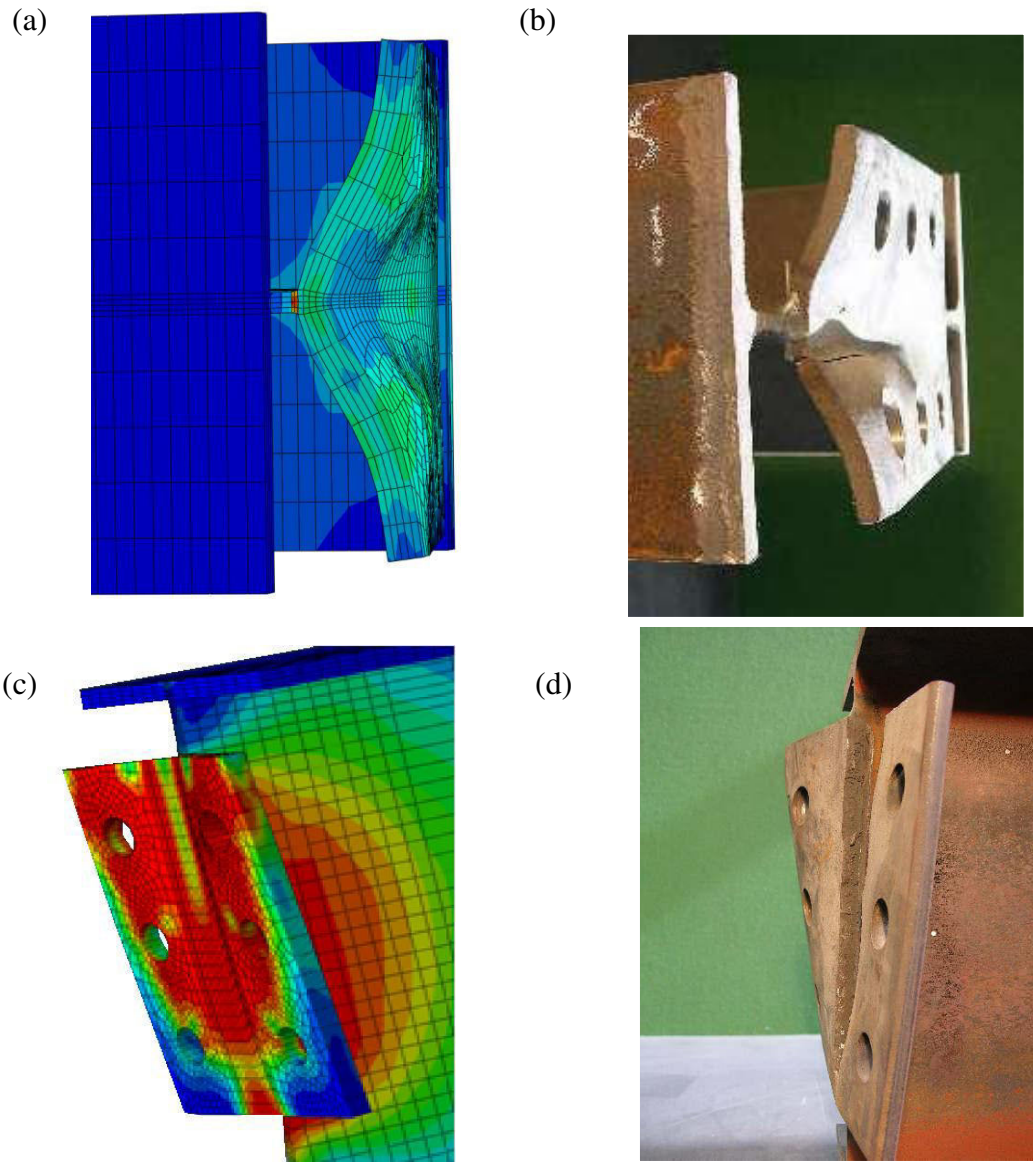


Fig. 4. (a) Deformed shape obtained from the FE simulation at 20° C (b) Experiment-deformed shape at 20° C [20] (c) Deformed shape obtained from the FE simulation at 550° C (d) Experiment-deformed shape at 550° C [20]

Table 1. Shear endplate capacities: comparison of experiments and FE simulations

Temp (°C)	Exp Max Load (kips)	FE Max Load (kips)	Failure Mode¹
	Inclined Tension		
20	43.16 (192 KN)	42 (185 KN)	Plate Rupture
450	20.31 (90.36 KN)	19.3 (86 KN)	Plate Rupture
550	15.4 (68.51 KN)	15 (66 KN)	Plate Rupture
650	6.39 (28.45 KN)	5 (22 KN)	Plate Rupture

¹ The tabulated failure modes correspond to the ones observed in the experiments (initial loading angle is 35° for 20°C, 450°C, 550°C, and the angle is 45° for 650°C) which also were predicted in the FE models.

CHAPTER III

SHEAR ENDPLATE CONNECTION ASSEMBLY: EVALUATIONS OF DEMAND

Shear endplate connections are generally designed to resist gravity loads only. However, in fire, large axial forces can develop in the beam and connection. To investigate the connection behavior in such conditions, a series of studies is conducted using 3D FE models in ABAQUS [19]. The overall goal is to gain further insight into major key parameters that impact the performance of beam-to-column shear endplate connections in a fire.

In the FE model, two limitations are considered. The analysis is unable to predict the connection performance after first component fracture; and the concrete floor system is not included in the models.

A series of FE models of typical floor beams with shear endplate connections are developed and analyzed. Parametric study is performed to examine the effects of several loading variables and boundary conditions on the behavior of shear endplate connections in fire. Also, a number of connection details that may affect the connection performance are investigated.

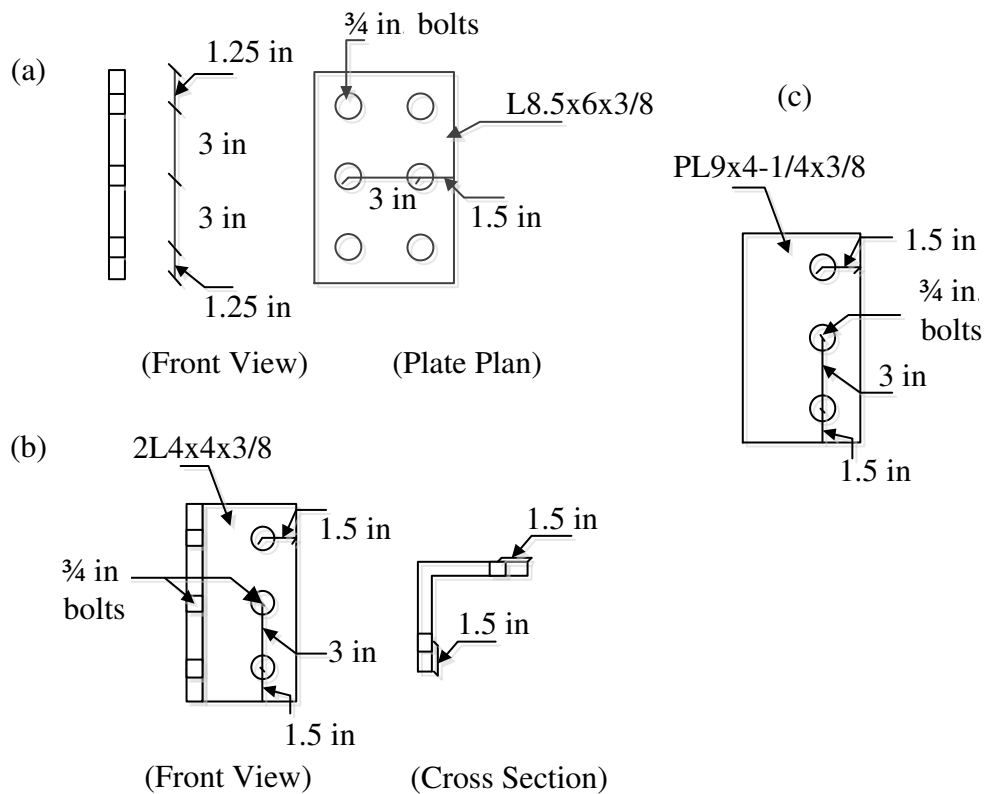
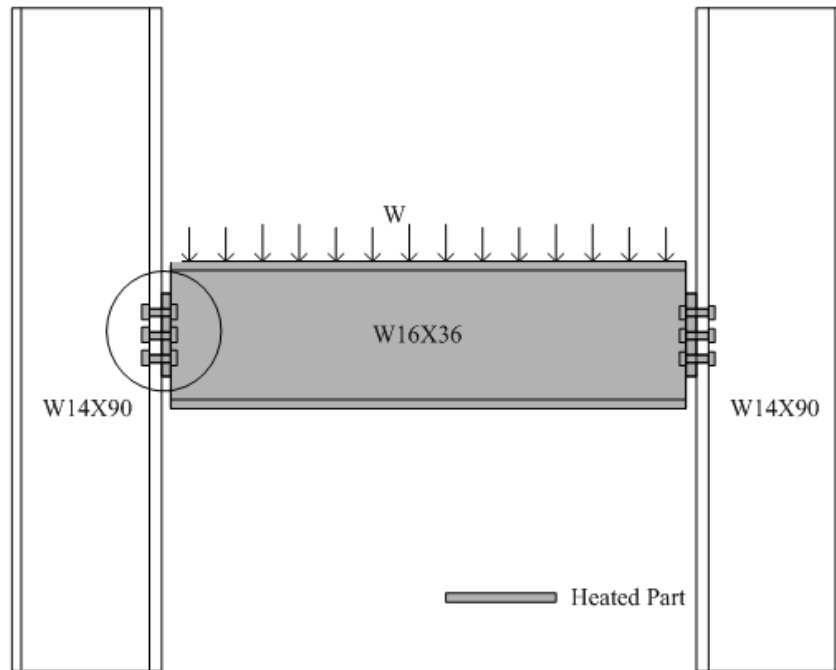


Fig. 5. Layout of connection assemblies used in parametric study. (a) Shear endplate connection, (b) Double angle connection, (c) Shear tab connection

A. Description of the Connection Assembly Model

A W16x36 floor beam spanning between W14x90 columns was used in the parametric study. The beam ends are attached to the columns using shear endplate connections welded to the beam web and bolted to the column flange, as shown in Fig. 5(a). The ambient temperature material properties for the structural bolts and steel materials that were used in the FE simulations are similar to the ones used by Hu and Engelhardt [8] in a previous study on shear tab connections. The column segments used in the model were 10 ft (3.05 m) long and assumed pinned at both the top and bottom ends. The shear endplate connection corresponding to W16x36 beam was designed for a gravity load that produces a moment equal to the plastic moment of the beam. ASTM A490 bolts were used in the model and the retention factors proposed by Eurocode 3 [24] were used to define the elevated temperature material properties of these bolts. The retention factors proposed by Lee et al. [22] were used to define the material properties of the base material at elevated temperature. A uniformly distributed load was applied to the beam. The magnitude of the distributed load was chosen to produce a maximum moment equal to a certain ratio of the plastic moment capacity of the beam at ambient temperature. Transient analysis was performed, which means that the applied load is held constant on the beam while temperature is changing. The beam and the shear endplate were heated as shown in Fig. 5(a). The remaining parts of the model were assumed to be insulated. The temperature was assumed to increase linearly with time and uniformly distributed in the heated parts of the structure. The temperature was increased to 650°C and then cooled down to 20°C.

B. Effect of Key Parameters and Connection Details

Several key parameters were studied including load ratio, beam length, initial cooling temperature, endplate location, and endplate thickness.

1. Load Ratio

The load ratio is defined as the ratio of the maximum moment developed in the beam to the nominal plastic moment capacity of the beam section M_p . In the parametric study, the beam is modeled as simply supported, and thus the maximum moment developed at midspan is equal to $wl^2/8$, where w is the applied load and l is the span length. The length of the beam is 30 ft (9.15 m), which is a typical span length encountered in buildings. The load ratios used in the analysis are 0.25, 0.5, and 1.0.

Fig. 6(a) shows the variation of axial force with temperature. It can be seen that when the load ratio is 1.0 (full plastification of the beam section), the maximum compressive force on the connection is significantly reduced when compared to the cases where the ratio is 0.25 and 0.5. This is due to the fact that the beam has already yielded and cannot develop any additional thermal induced compressive forces. In addition, for the case when the load ratio is 1.0, yielding mechanism in the shear endplate occurred. Thus, the connection could not carry the total axial force developed during the heating stage, and failure occurred at 310°C. When increasing the load ratio from 0.25 to 0.5, no significant variation of the connection axial force during either heating or cooling stages was observed. Also, the analysis shows that a higher load ratio produces less compression force in the beam but higher tension force when catenary action develops.

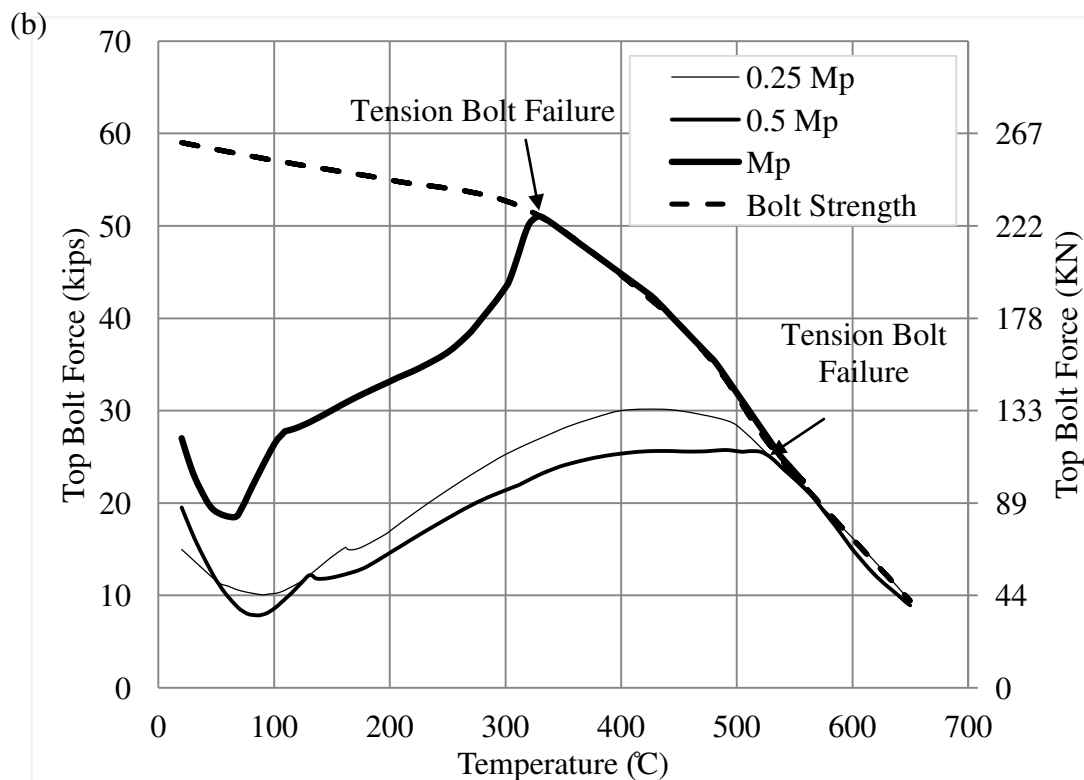
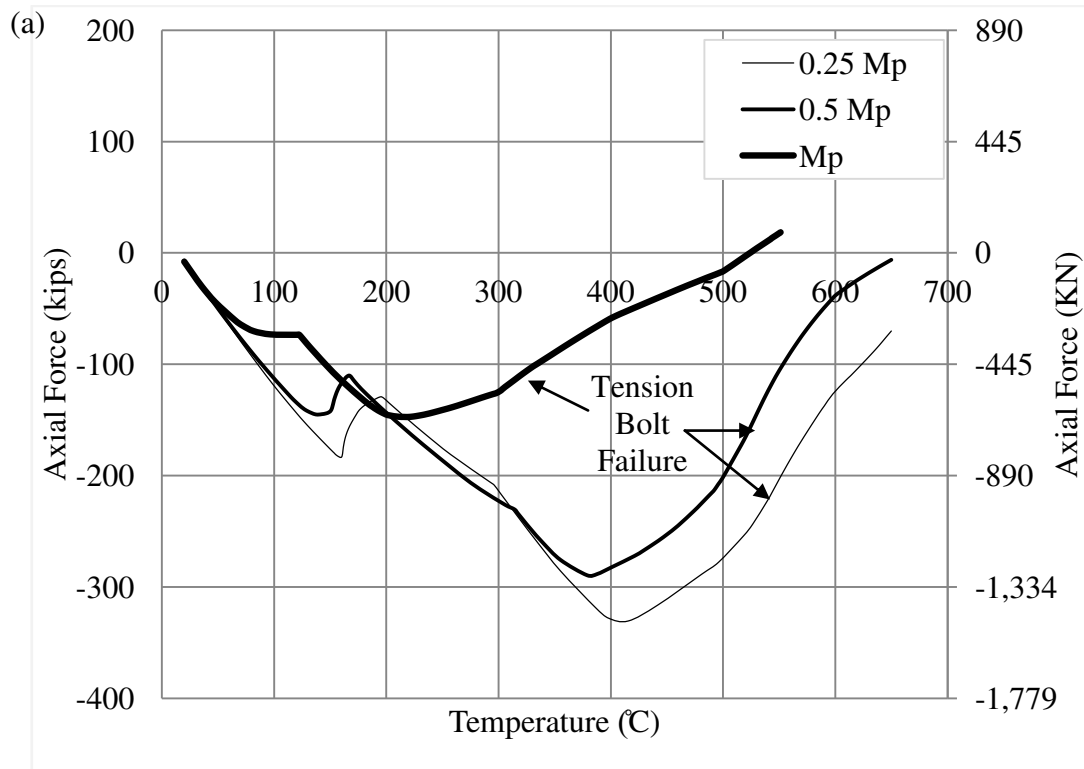


Fig. 6. (a) Axial force in the shear endplate during heating and cooling for a varying load ratio, (b) Top bolt force comparison during heating for a varying load ratio (Solid lines are heating; dashed lines are cooling)

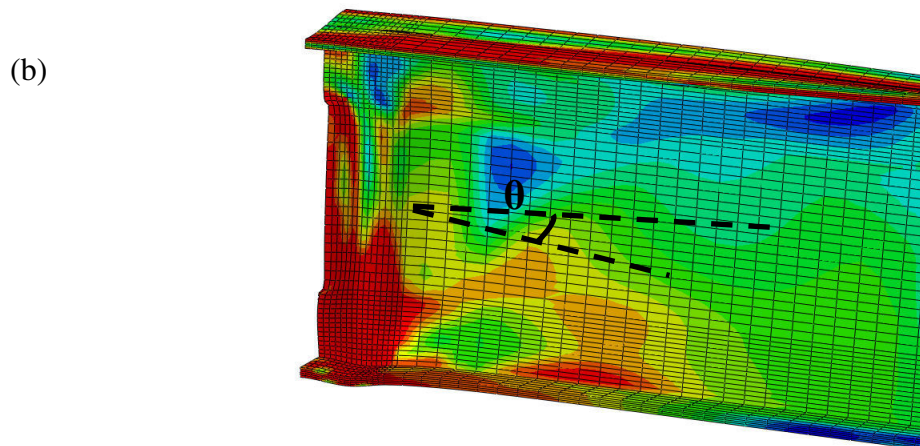
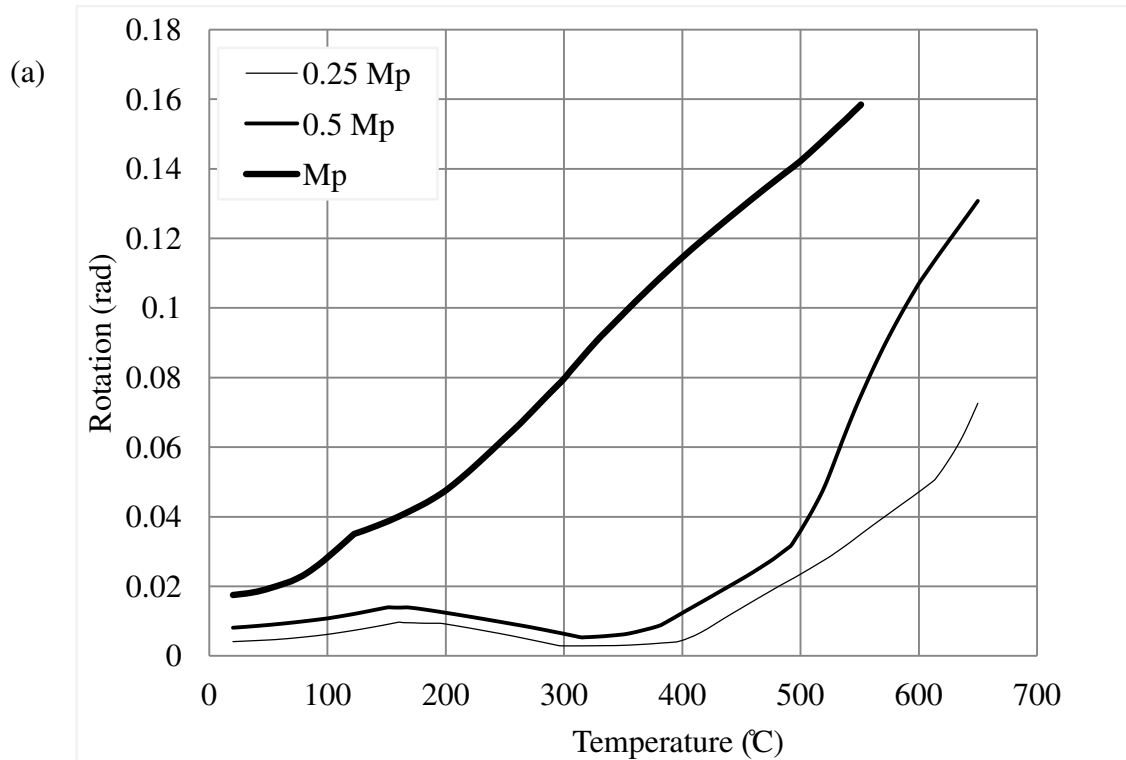


Fig. 7. (a) Beam rotation for varying load ratios (W16), (b) Definition of beam rotation

Fig. 6(b) shows the top bolt force with temperature for different load ratios. In all three cases, tension bolt failure occurs in the heating stage. Also, it can be seen that for the case of load ratio is equal to 1, bolt failure occurred at 310°C. However, for the case of load ratio 0.25 and 0.5, bolt failure occurred around 560°C.

Fig. 7(a) shows the connection rotation for different load ratios. Note that the rotation is defined in this study as the change in angle formed by the centerline of the

beam web as shown in Fig. 7(b). Fig. 8 shows the connection uplift with different load ratios versus temperature. The endplate uplift is defined as the separation of the endplate from the column flange. It can be seen that the connection uplift and rotation increase as the load ratio increases.

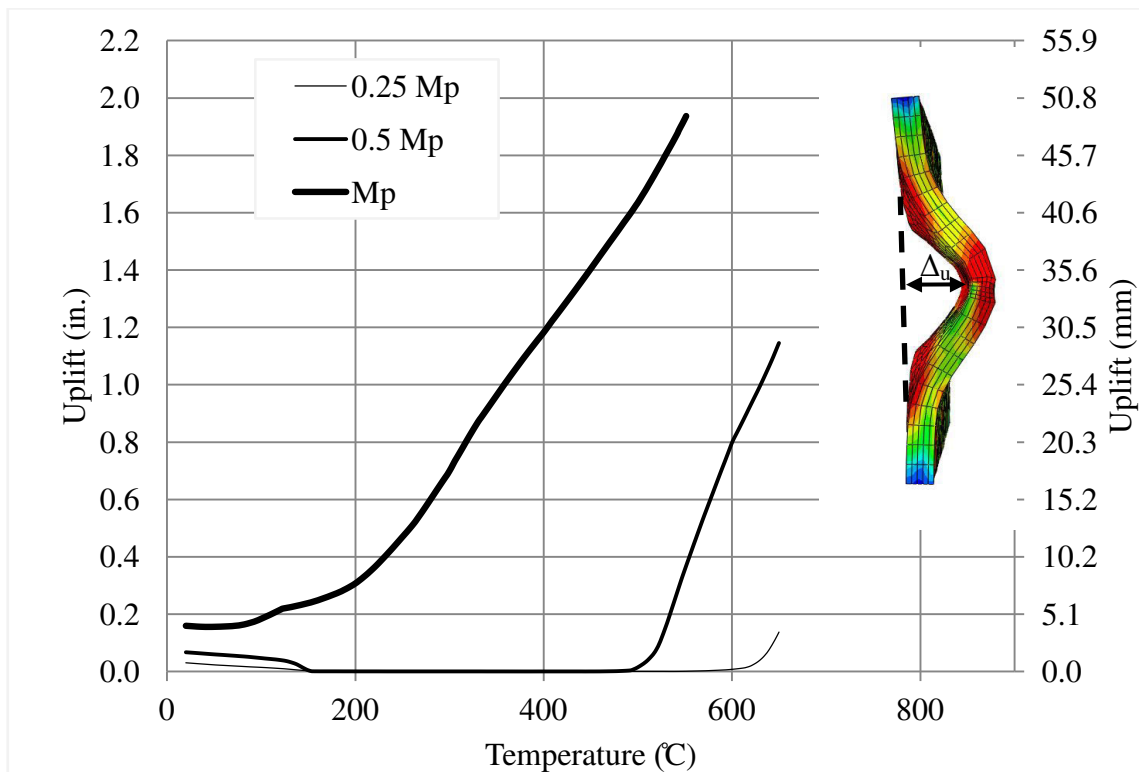


Fig. 8. Endplate uplift for varying load ratios (W16)

In conclusion, increasing the load ratio limits the maximum axial compressive force in the beam. Nevertheless, it can cause early tension bolt failure and yielding of the endplate.

2. Beam Length

A study on the effect of beam length on the connection behavior in fire is performed. Beams having 20 ft (6.10 m), 30 ft (9.15 m), and 40 ft (12.20 m) length were selected for analysis. For all beams, the load ratio was chosen to be 1/3.

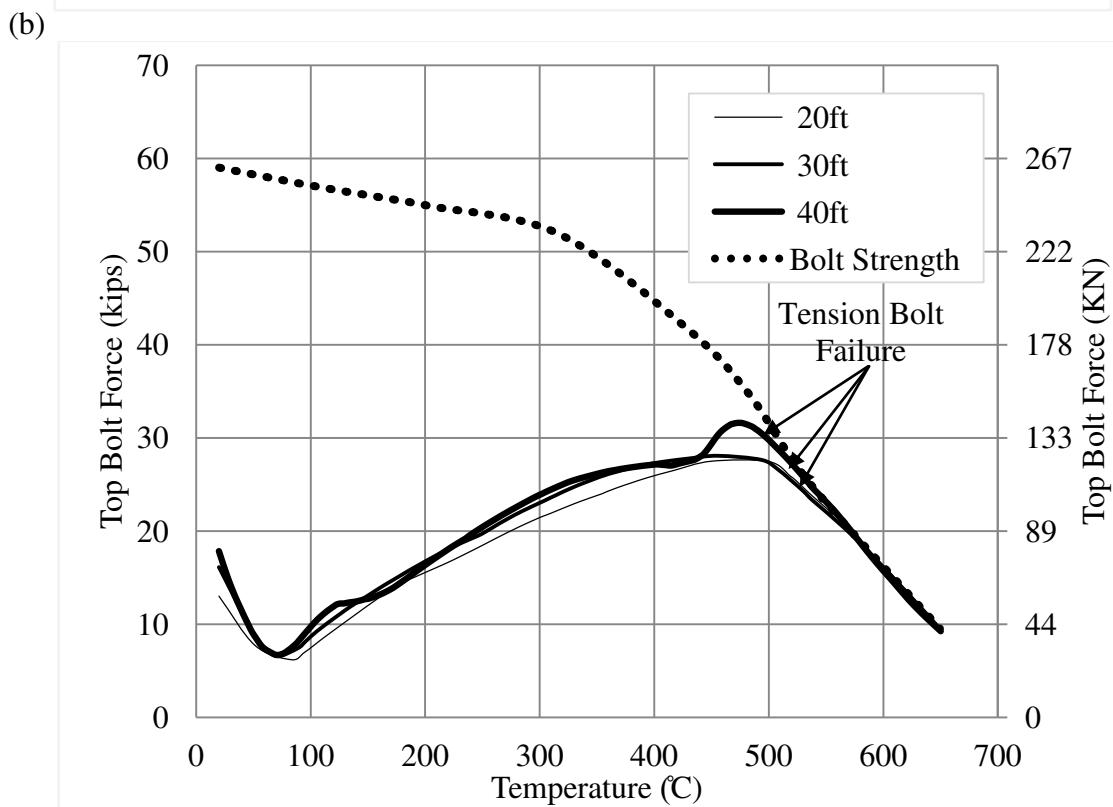
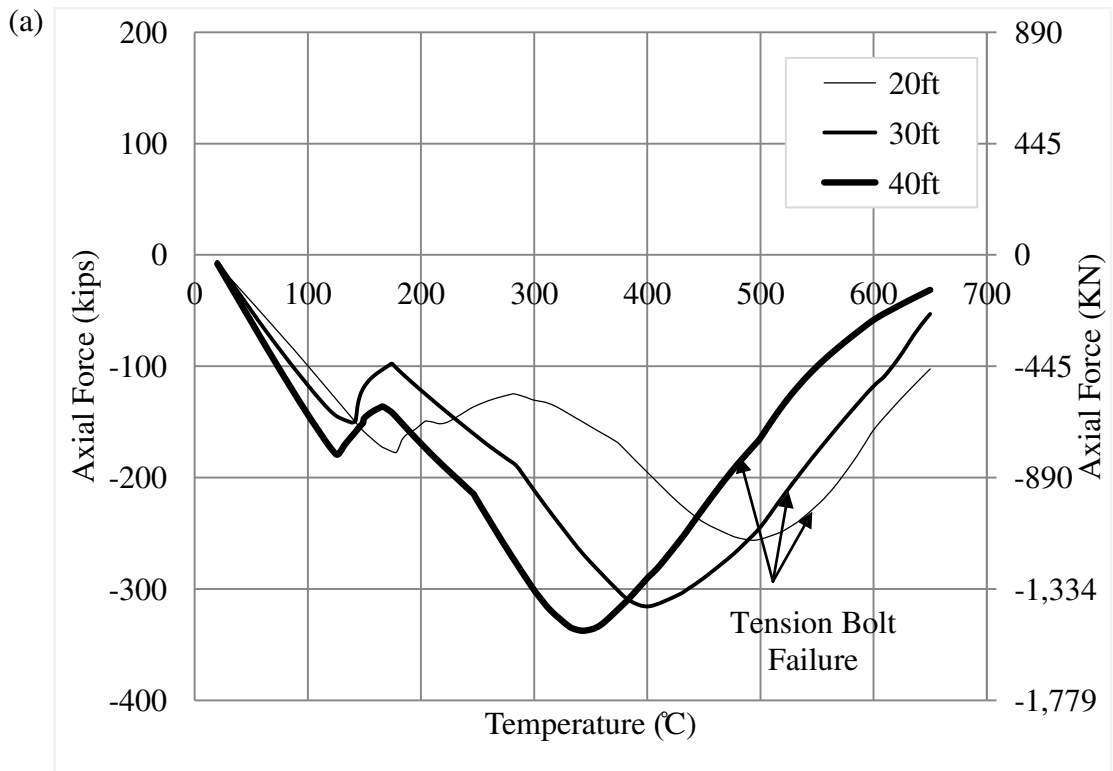


Fig. 9. (a) Axial force in the shear endplate for varying beam lengths (W16),
 (b) Top bolt force comparison for varying beam lengths (W16)

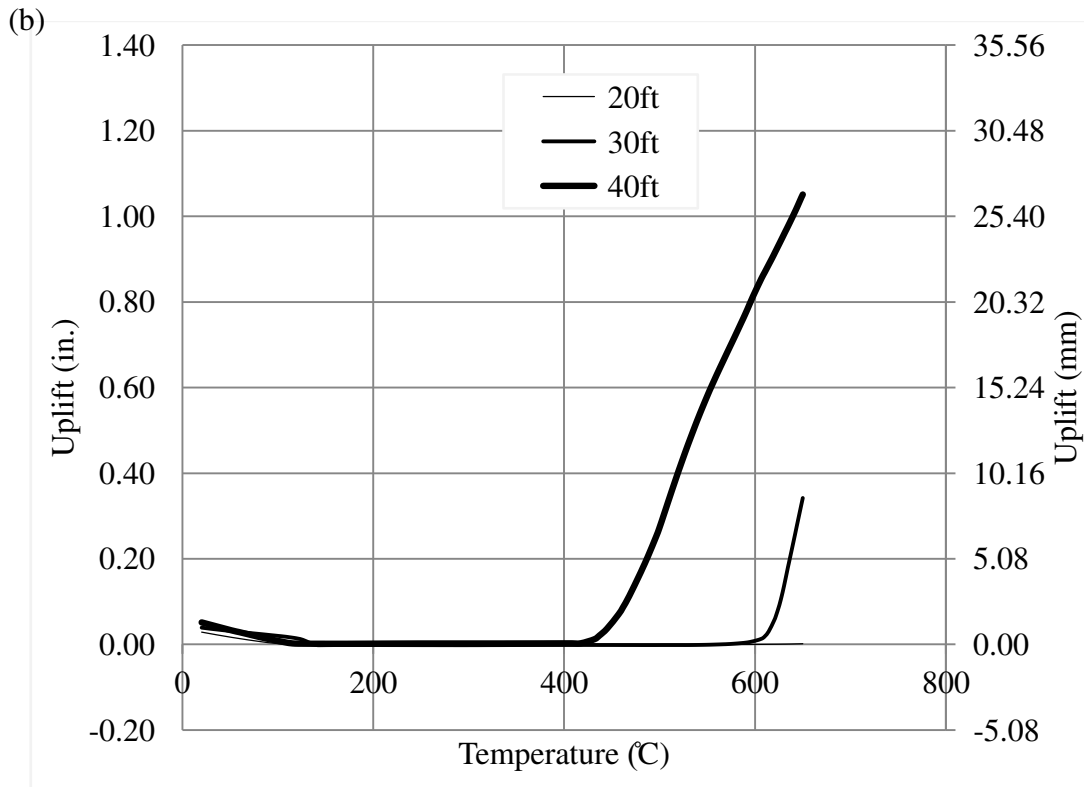
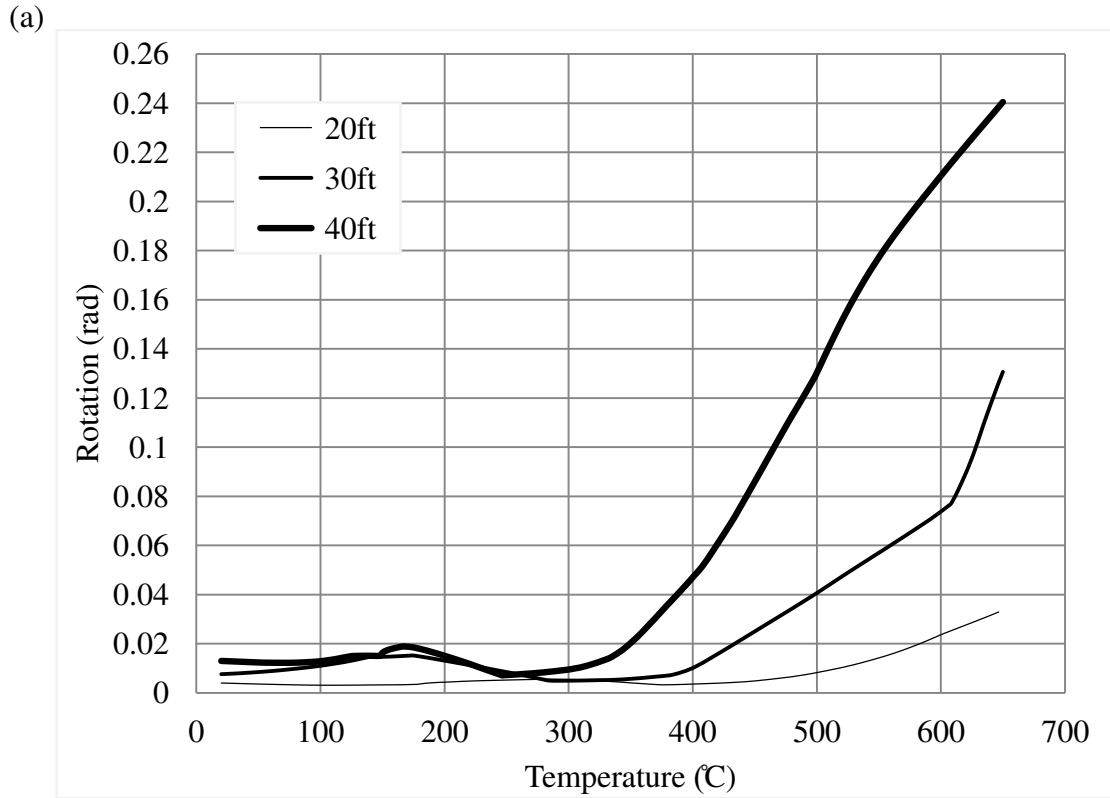


Fig. 10. (a) Beam rotation for varying beam lengths (W16), (b) Endplate uplift for varying beam lengths (W16)

Results are plotted in Figs. 9 and 10. The FE results show that although longer beams develop higher compressive force, the maximum axial compressive force on the connection for longer beams occurs at a lower temperature (Fig. 9(a)). Fig. 9(b) shows the variation of the top tension bolt force versus temperature, respectively. It can be seen that for the 40 ft (12.20 m) beam, tension bolt failure occurs at about 490°C while tension bolts in the other connections with beam length of 20 ft (6.10 m) and 30 ft (9.15 m) fail at 550°C. Figs. 10(a) and 10(b) show the connection rotation and uplift versus temperature. It can be seen that the longest beam has a lower rotational stiffness, and thus produces higher connection rotation and uplift.

In conclusion, the beam length affects the behavior of connection, where a longer beam develops a higher maximum axial compressive force and an earlier tension bolt failure.

3. Initial Cooling Temperature

The initial cooling temperature is defined as the highest temperature reached in a fire event. To study the effect of this parameter on the behavior of the shear endplate connection, four 30 ft (9.15 m) beams with a load ratio of 0.5 are used. The beams are heated up to 400°C, 500°C, 600°C and 650°C respectively, and then cooled down to 20°C.

Fig. 11(a) shows the axial force in the connection versus temperature. It can be seen that higher initial cooling temperature produces larger axial tensile force during cooling. In addition, Fig. 11(b) shows that for an initial cooling temperature of 500°C or less, no tension bolt failure occurs. This can be due to the additional loss of stiffness that occurs in the beam and connection as the temperature increases.

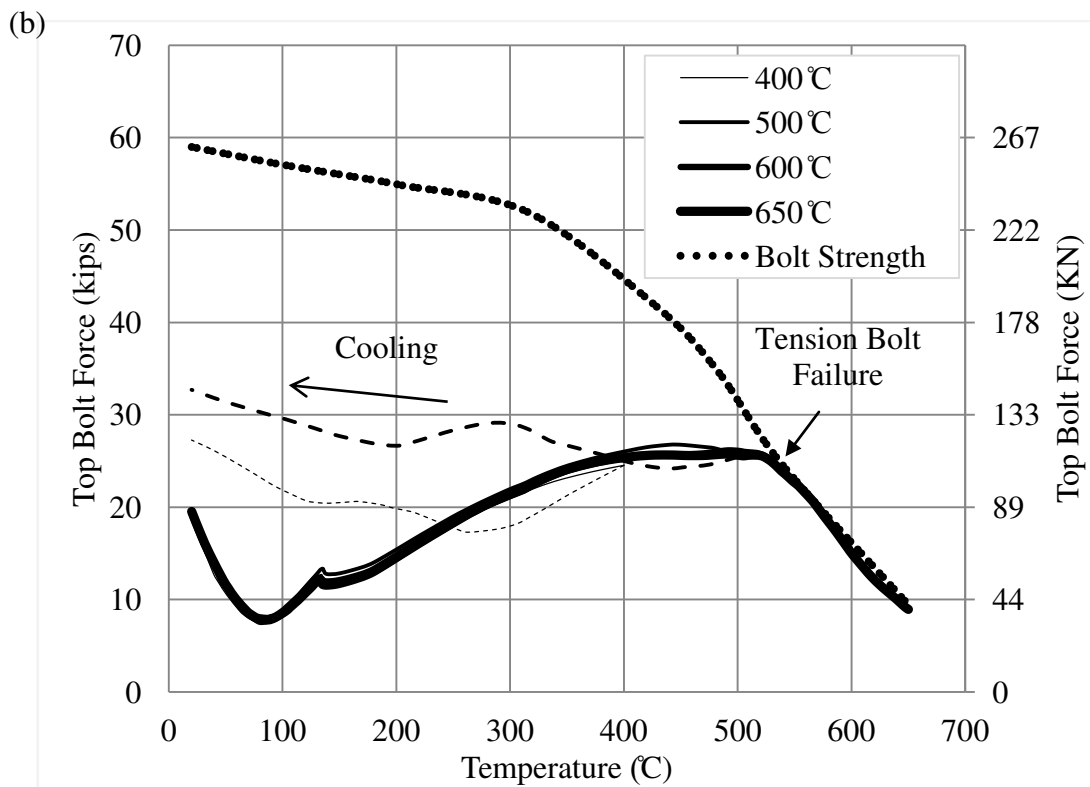
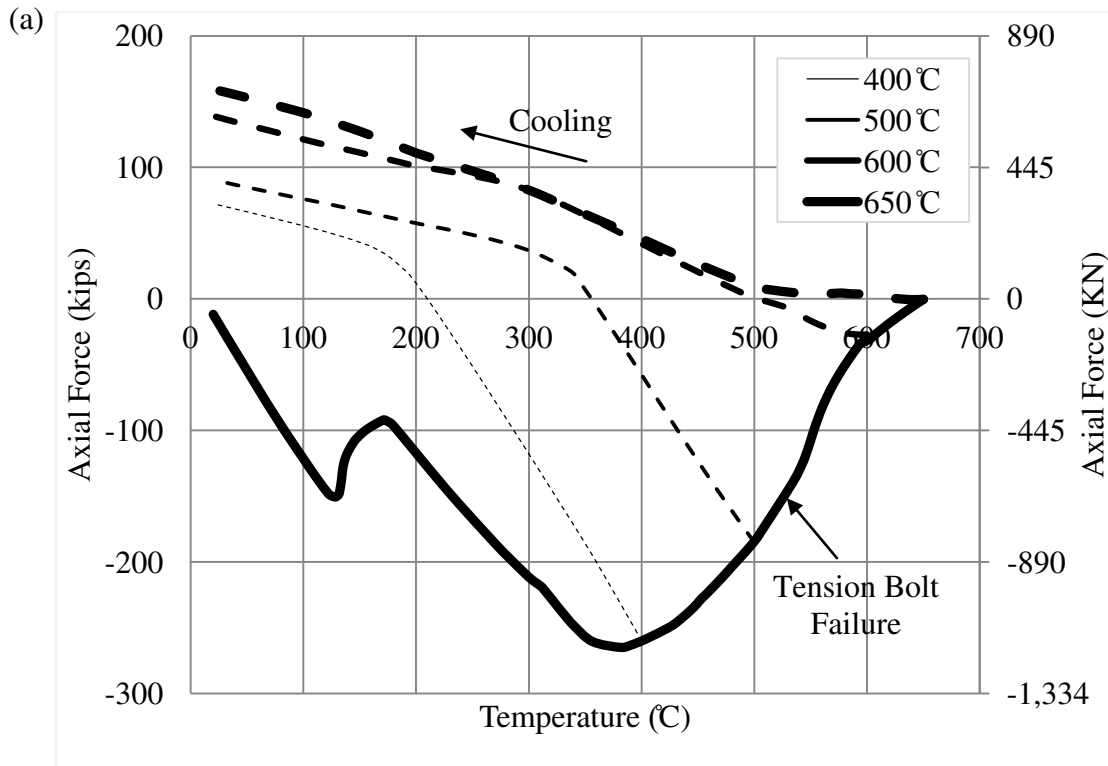


Fig. 11. (a) Axial force in the shear endplate for varying initial cooling temperatures (W16), (b) Top bolt force comparison for varying initial cooling temperatures (W16)

It can be concluded that for an initial cooling temperature of 500°C or less, no failure occurs, and the maximum compressive axial load is lower than for the case where the initial cooling temperature is 600°C or 650°C.

4. Shear Endplate Location

Another parameter that is considered in the study is the shear endplate location. To investigate the effect of this connection detail on the overall performance, three cases are analyzed. The selected endplate locations are (1) at mid height of the beam web, (2) at 1.25 in (3.2 cm) above mid height of the beam web, and (3) at 2.75 in (7 cm) above mid height of the beam web. The beam is 30 ft (9.15 m) long with a load ratio of 0.5. The axial force versus temperature is shown in Fig. 12. It can be seen that the plate location has no effect on the behavior of the connection.

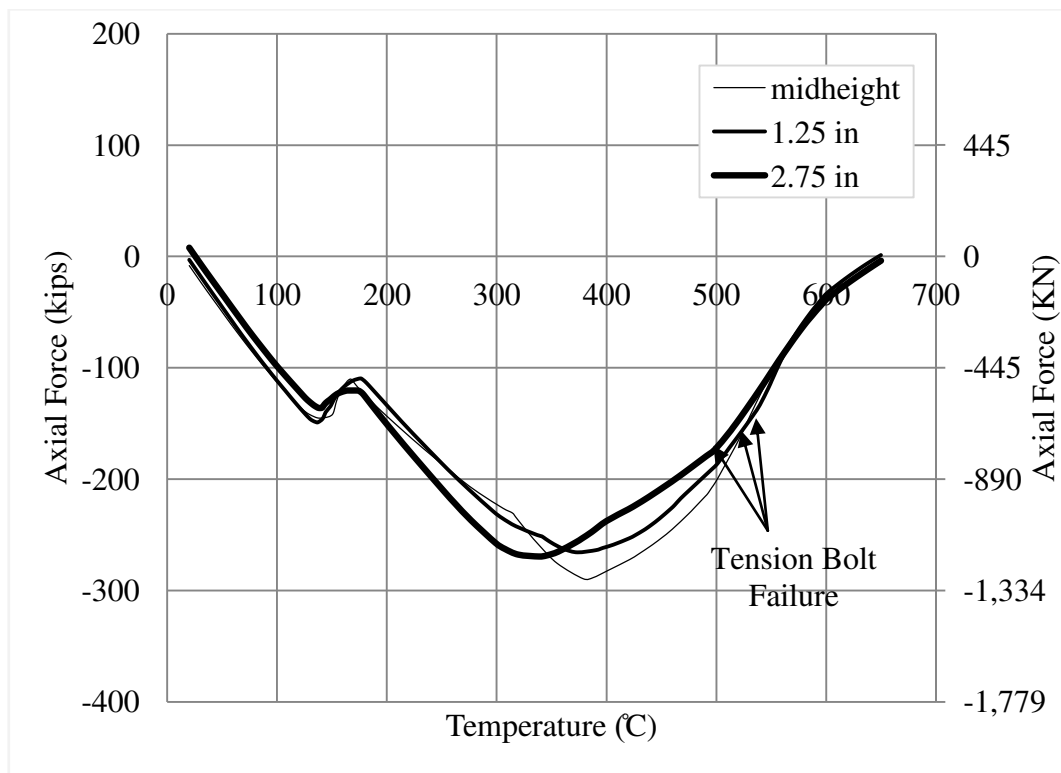


Fig. 12. Axial force in the shear endplate for varying endplate locations (W16)

5. Shear Endplate Thickness

Another parameter included in this study is the plate thickness. To study the effect of this parameter on the connection behavior, two different thicknesses are considered: 0.375 in (1 cm) and 0.5 in (1.3 cm). The beam is 30 ft (9.15 m) long with a load ratio of 0.5.

Fig. 13 shows the variation developed axial force in the connection for different endplate thicknesses. It can be seen that the maximum compressive force is greater for the 0.375 in (1 cm) thick plate.

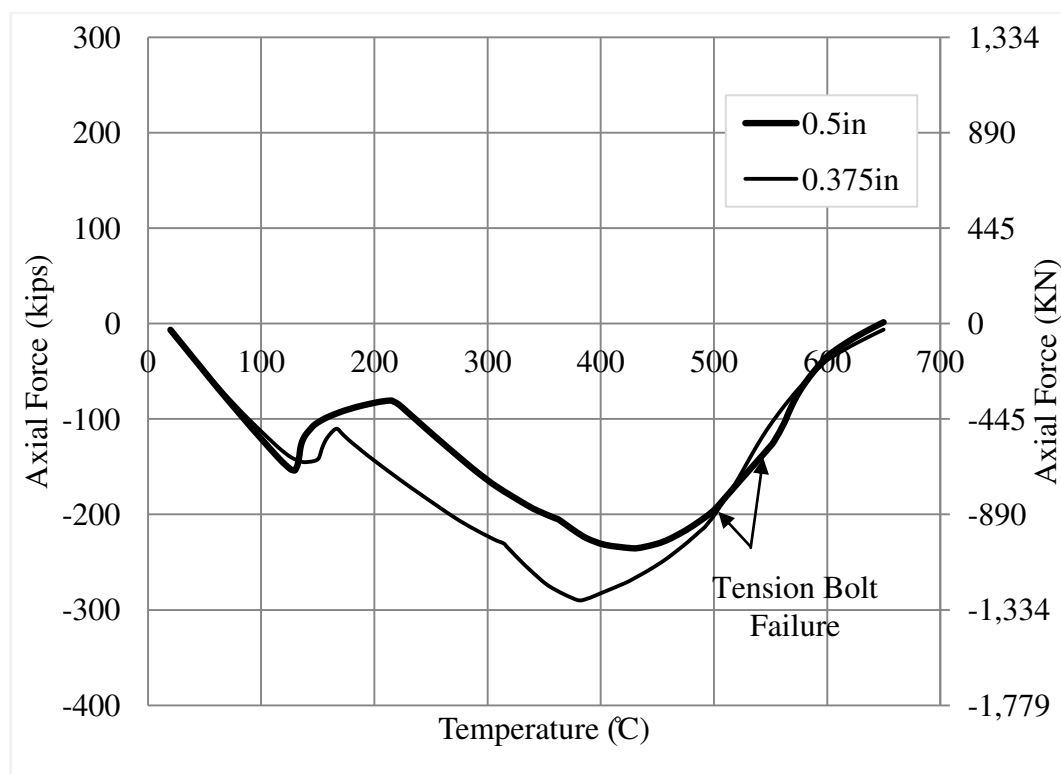


Fig. 13. Axial force in the shear endplate for a varying endplate thickness (W16)

Figs. 14(a) and 14(b) show the beam rotation and connection uplift for different endplate thickness. It can be deduced that decreasing the endplate thickness increases the plate uplift.

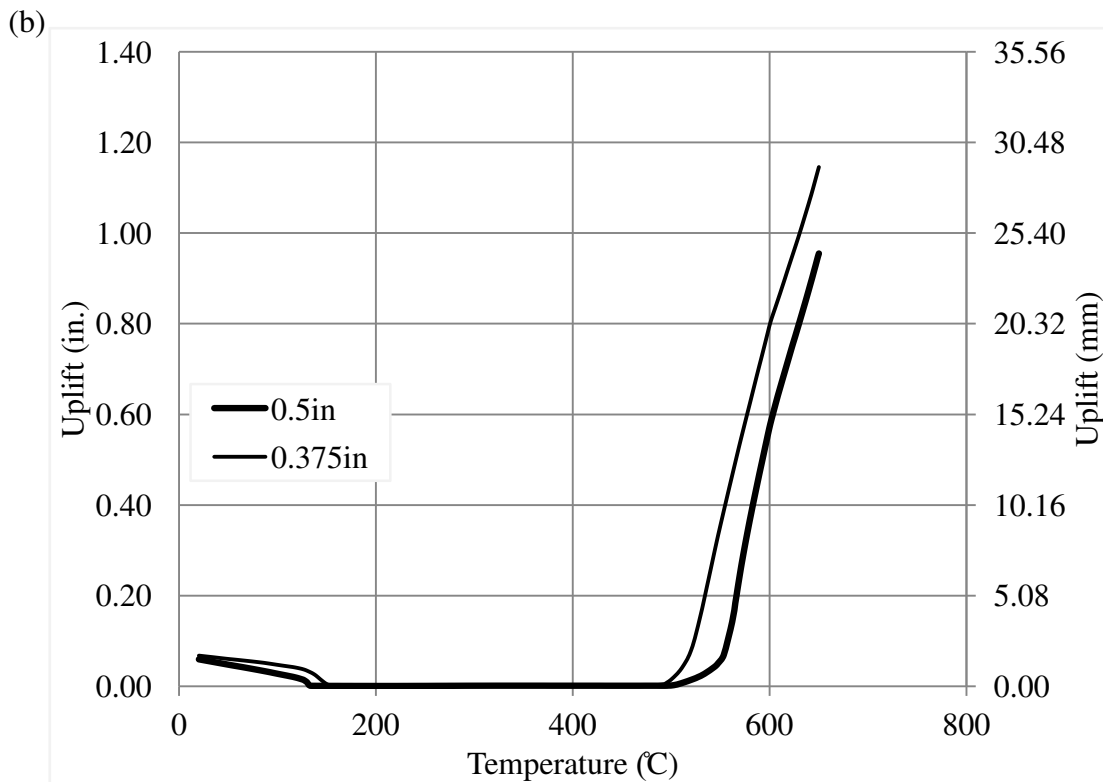
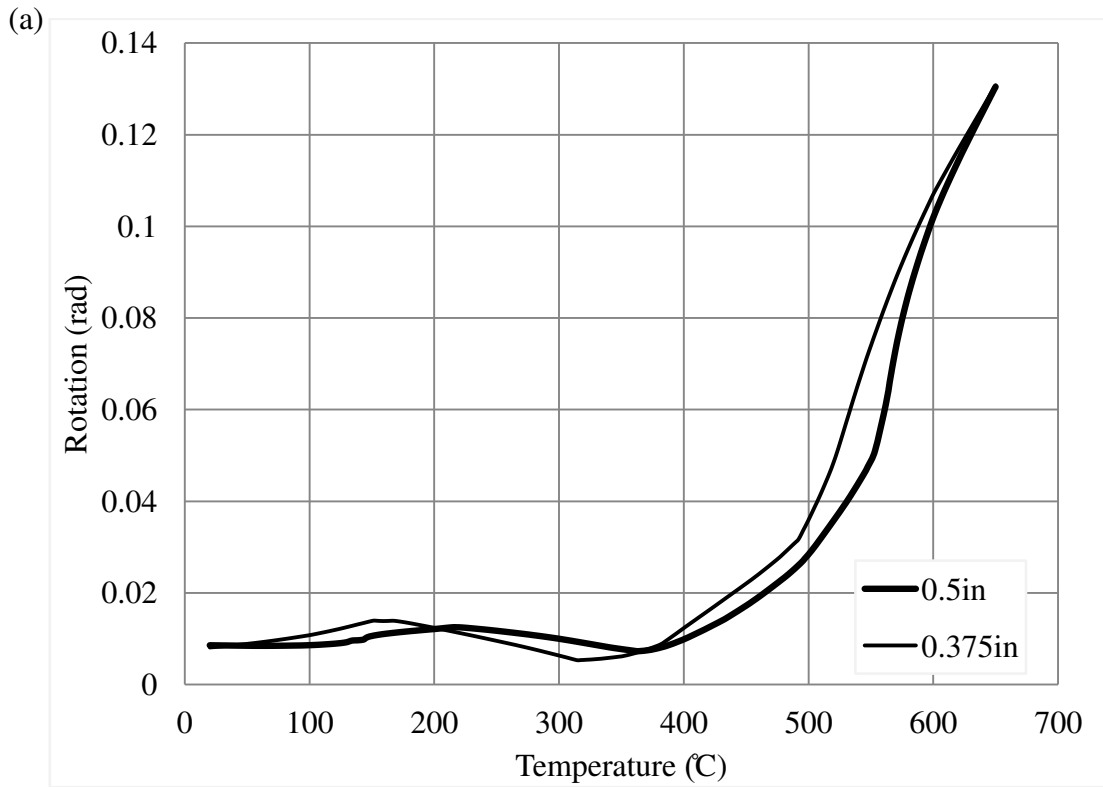


Fig. 14. (a) Beam rotation comparison for different endplate thicknesses (W16), (b) Endplate uplift for a varying endplate thickness (W16)

6. Beam Depth

A study on the effect of the beam depth is made. The considered cases are W16x36 and W18x46 with a beam length of 30 ft (9.15 m) for both. The other connection dimensions are the same and the load ratio is 0.5. Fig. 15 shows that the maximum compressive axial force is greater for the deeper beam. The tension bolts fail at 520°C. It can be seen from the parametric study that the thermally induced axial force in the beam is affected by the load ratio, beam length, and shear endplate thickness. These parameters are used later in the formulation of the mechanistic model for the shear endplate connection behavior in fire.

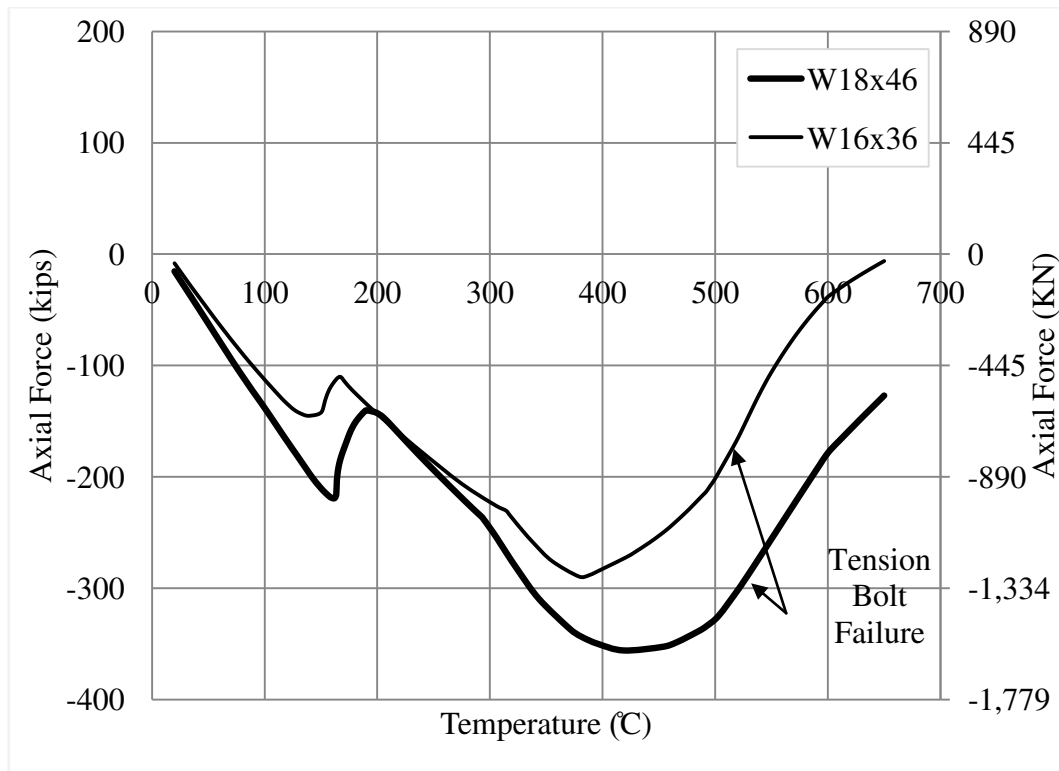


Fig. 15. Axial force in the shear endplate for a varying beam depth,

CHAPTER IV

COMPARISON OF SHEAR ENDPLATE, SHEAR TAB AND DOUBLE ANGLE CONNECTION ASSEMBLIES

This section provides a comparison of the behavior of the shear endplate, shear tab, and double angle connections under similar temperature histories. The shear tab and double angle connection assemblies were according to Hu and Engelhardt [8] and Hantouche et al. [18], respectively. The connections were associated with a 30 ft (9.15 m) long W16x36 beam with a load ratio of 0.5. The material model used for the shear endplate connection was described in the previous section. Figs. 5(a), 5(b), and 5(c) describe the details of the connections configurations of all three connections. The response of the shear endplate connection was compared to that of the shear tab and double angle [18].

Fig. 16(a) compares the axial force demands on the three connections. It can be seen that the rate of the axial compressive force increase at the beginning of the heating phase is the same for all connections. The maximum axial compressive force in the shear tab connection is controlled by plate and beam web local buckling at 80°C. Upon contact with the column at 450°C, the axial force increases again until beam flange buckling occurs at 530°C. For the shear endplate, the increase of the compressive axial force is first controlled by beam web buckling at 130°C. When contact occurs with the column at 160°C, the compressive axial force in the shear endplate increases to reach its maximum value at 380°C when lower beam flange buckling occurs. As for the double angle, the maximum compressive axial force occurs at about 230°C (web yielding) after local web buckling occurs at 130°C. No contact between the beam and column occurs in the double angle connection. The comparison

shows that the shear endplate connection carries the highest axial compressive force demand while the shear tab shows the lowest compressive demand during the heating phase. As the temperature keeps increasing, significant loss of strength and stiffness leads to a decrease in the axial compressive force in all three connections. As this loss of stiffness becomes significant at the end of the heating phase, sagging of the beam increases which leads to the development of axial tensile forces on the connections due to catenary action. At the end of the heating phase, the axial force on the connections has almost the same magnitude. During the cooling phase, no significant difference is observed between the double angle. The failure temperatures and modes of the three types of connections are summarized in Table 2.

Fig. 16(b) shows the beam rotation for all three connections. It can be seen that the double angle connection rotation increases at the highest rate. This is due to the fact that the flange uplift in the double angle provides additional deformation. The shear endplate rotation initially increases at the same rate until beam web buckling occurs at 150°C. The connection rotation then decreases until contact occurs. After contact, the rotation starts to increase significantly after beam flange buckling. During the cooling phase, the rotation in all three connections decreases at the same rate.

Fig. 17(a) shows a comparison of the bolt force in the top shear bolt with temperature for the double angle and shear tab connection. It can be seen that the bolt force in the top shear bolt associated with the shear tab is larger in magnitude than that associated with the double angle connection. This is due to the fact that in the case of the double angle, the shear force which is transferred to each shear bolt is distributed on two shear planes, whereas in the case of the shear tab it is distributed on one shear plane. In addition, for the shear tab connection, the shear force in the shear bolts

increases significantly during the cooling phase, and the bolts fail at a temperature of 230°C. However, no failure occurred in the shear bolts for the double angle connection.

Fig. 17(b) shows the top tension bolt force for the double angle and shear endplate connections. It can be seen that the top tension bolt fails in the shear endplate at 450 °C while no failure occurs in the double angle connection. Note that all the tension bolts in the shear endplate connection fail in the heating phase. This is due to the large axial force that develops in the connection.

The comparison between the three connections shows that the double angle is the least vulnerable to failure, the governing failure mode of the shear tab is shear bolt failure in the cooling phase while tension bolt failure of the shear endplate connection occurred in the heating phase.

Table 2. Failure modes and temperatures for the shear endplate, double angle, and shear tab connections

	Shear Endplate	Double Angle	Shear Tab
Failure Mode	Tension Bolt Failure	No Failure	Shear Bolt Failure
Failure Temperature	450°C	-	230°C
Fire Phase	Heating	-	Cooling

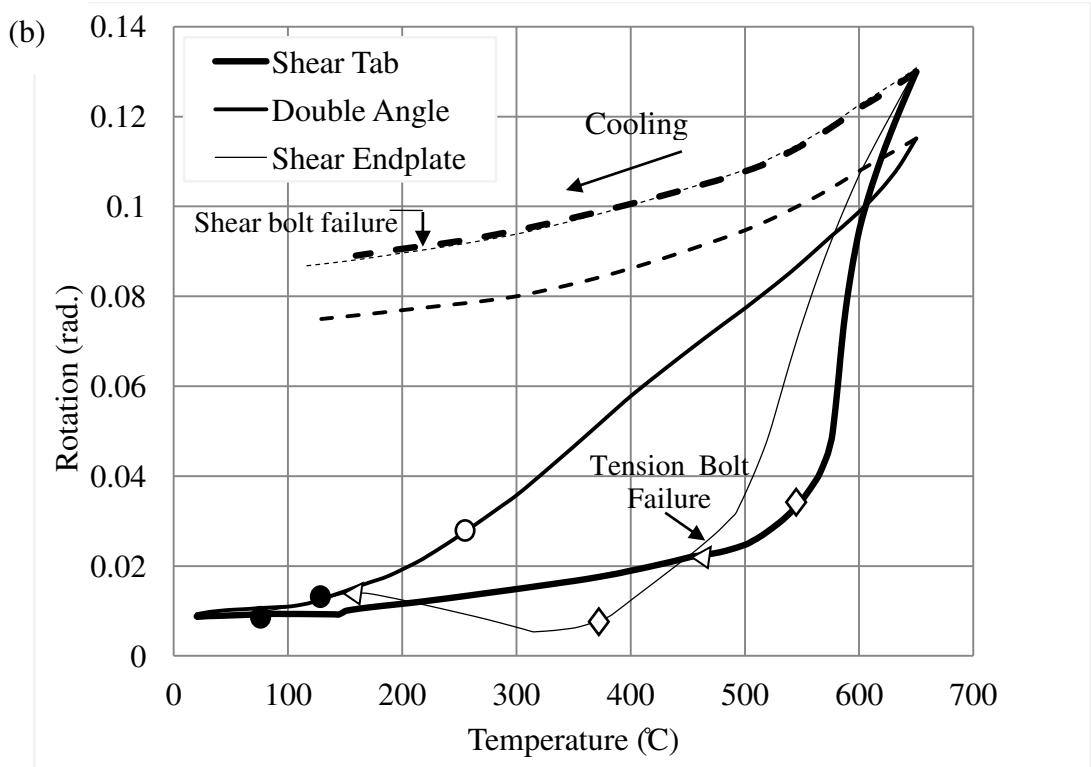
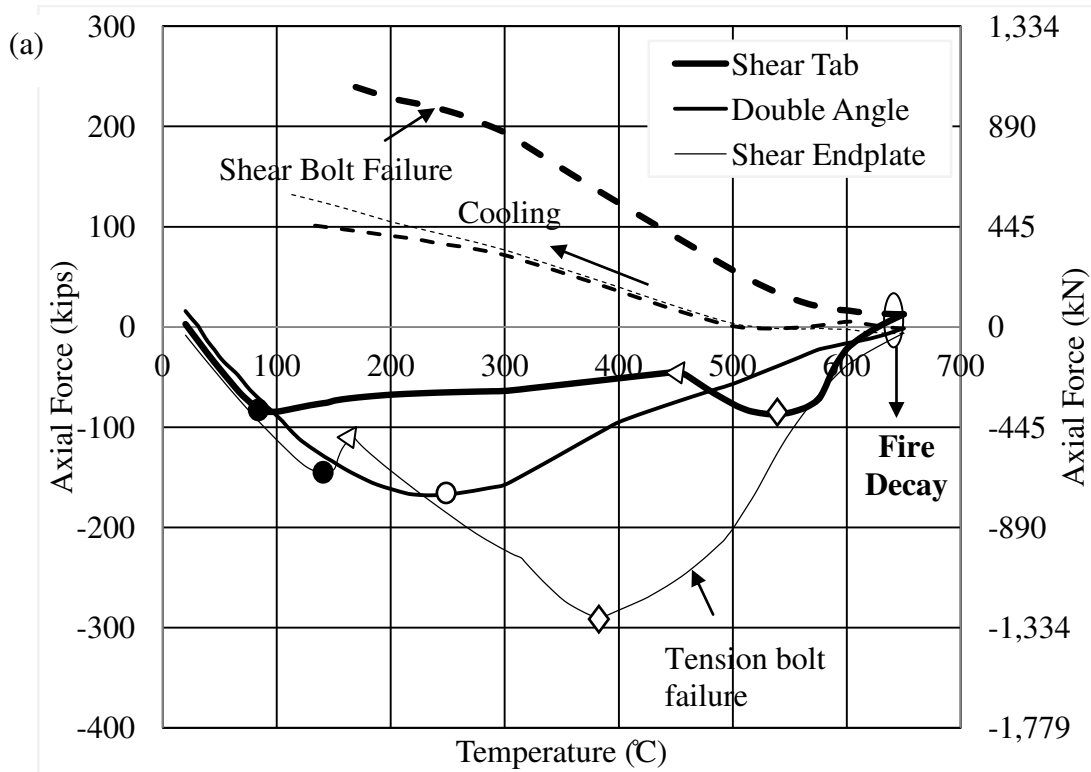


Fig. 16. (a) Axial force in the shear tab, double angle, and shear endplate connections, (b) connection rotation for the shear tab, double angle, and shear endplate connections (● - onset of beam web local buckling, ◁ - onset of flange contact, ○ - onset of beam web yielding, ◇ - onset of beam flange local buckling)

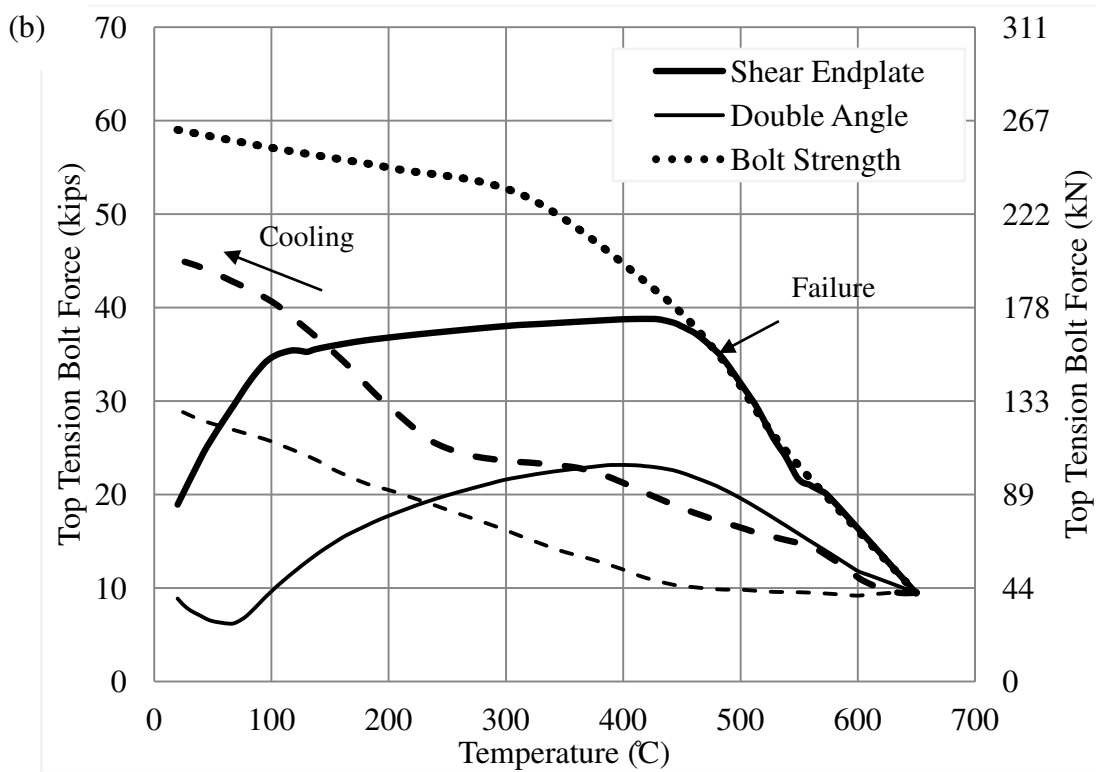
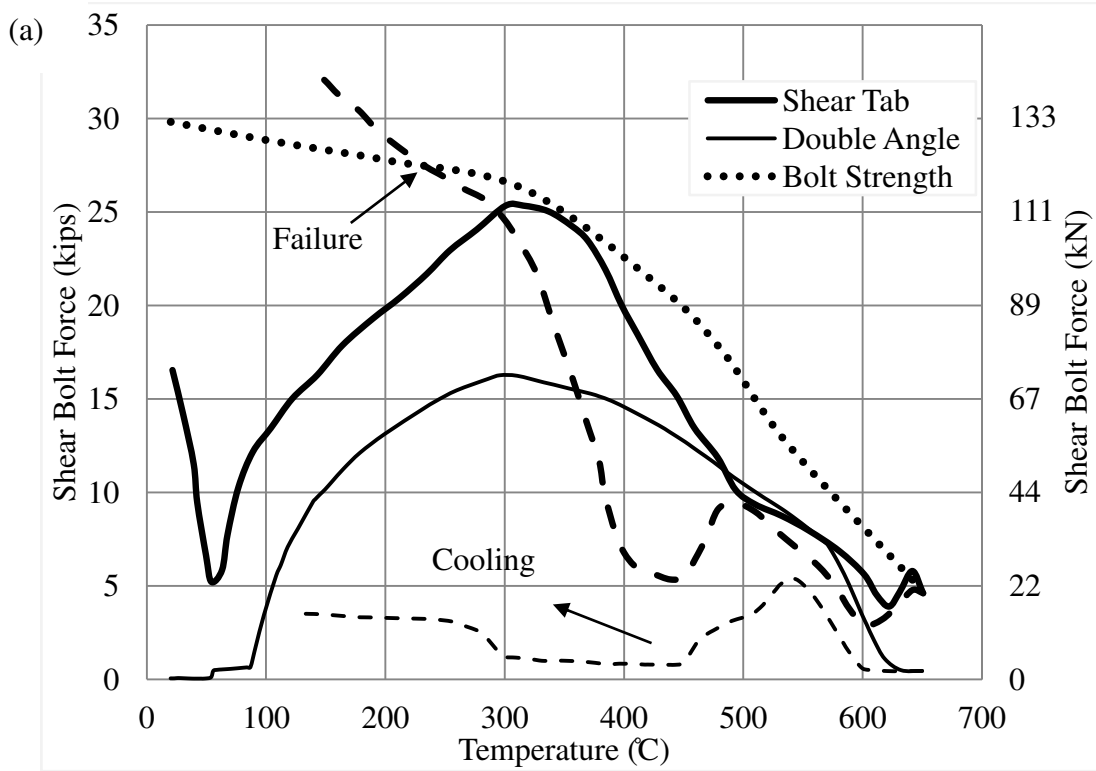


Fig. 17. (a) Comparison of shear bolt force in the shear tab and double angle, (b) Comparison of the top tension bolt force for the double angle and the shear endplate connections

CHAPTER V

MECHANISTIC MODELING FOR PREDICTING THE THERMAL-INDUCED AXIAL FORCES OF SHEAR ENDPLATE CONNECTIONS IN FIRE

Current U.S. building standards for structural fire resistance do not explicitly consider beam-to-column connections. During a fire, thermal induced axial forces will develop in the beam and connection parts due to the axial restraint provided by the connection. These axial forces are first compressive, and then become tensile when the structure loses stiffness and catenary action starts at a later stage of the heating during a fire.

The FE results show two types of mechanism of the beam-shear endplate connection (i) buckling of the beam web and lower flange which occurs at a load ratio less than 0.85 (Type I), and (ii) yielding of the beam web and lower flange which occurs at a load ratio greater than 0.85 (Type II). Figs. 18(a) and 18(b) show a nonlinear behavior of the variation of the axial force with temperature in the beam-shear endplate connection for type I and type II mechanisms, respectively.

The parameters considered in the formulation of the proposed models are: beam length, endplate thickness, load ratio, column depth, column web thickness, and beam cross-sectional area.

The proposed model allows design engineers to quantify the thermal induced forces and to predict the axial force versus temperature of beam-shear endplate connection during a fire event.

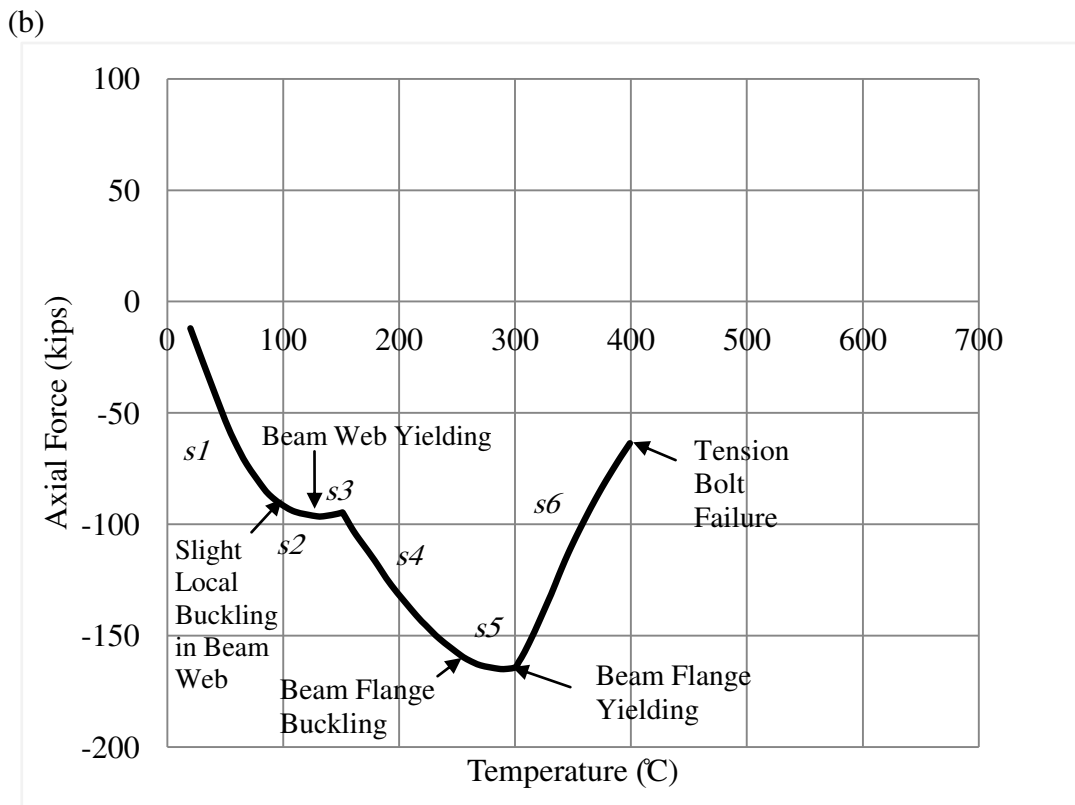
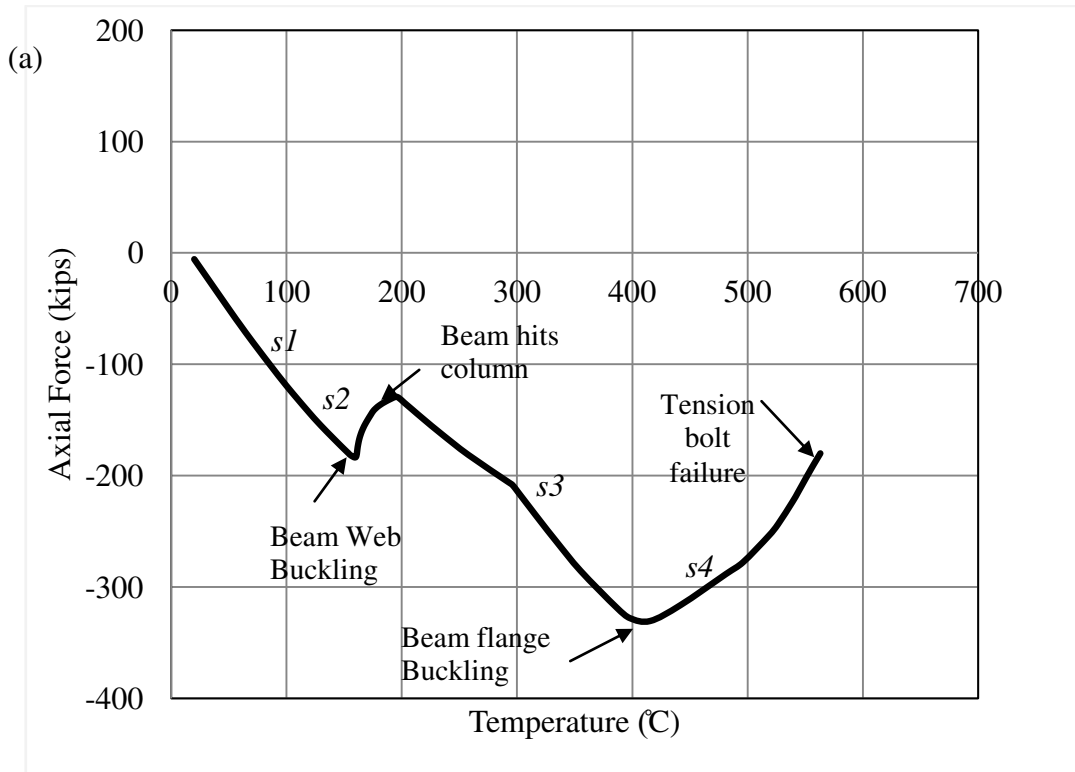


Fig. 18. Typical variation of the axial force with temperature for a shear endplate connection, (a) type I, (b) type II

A. Description of the Behavior:

1. Proposed Model I

Fig. 18(a) describes the thermal induced axial forces in the beam at elevated temperature. The behavior is divided into four segments during the heating phase of the fire. As the temperature increases, the compressive axial force in the beam increases until the beam web buckles (*s1*). The axial load starts decreasing due to buckling of the beam web (*s2*). At the onset of contact of the beam flange and column flange, the axial force increases until it reaches a maximum value where beam flange buckling occurs (*s3*). At a certain temperature, an increase in beam deflection is accompanied by catenary action development in the beam (*s4*). The compressive axial force drops gradually and tension bolt failure occurs.

2. Proposed Model II

Fig. 18(b) describes the thermal induced axial forces in the beam at elevated temperature. As the temperature increases, the compressive axial load in the beam increases until local web buckling occurs in the beam followed by beam web yielding (*s1*, *s2*, and *s3*). When contact occurs between beam flange and column flange, the axial force increases until it reaches a maximum value when local beam flange buckling occurs followed by beam flange yielding (*s4* and *s5*). The yielding of the beam flange limits the compressive axial force. The compressive axial force drops gradually, and at a certain temperature, an increase in deflection accompanied by catenary action that develops in the beam leads to tension bolt failure (*s6*).

B. Elastic and Plastic Stiffness of the Connection

The beam is modeled using a beam element and the connection and column parts are modeled using an axial spring as shown in Fig. 19(a).

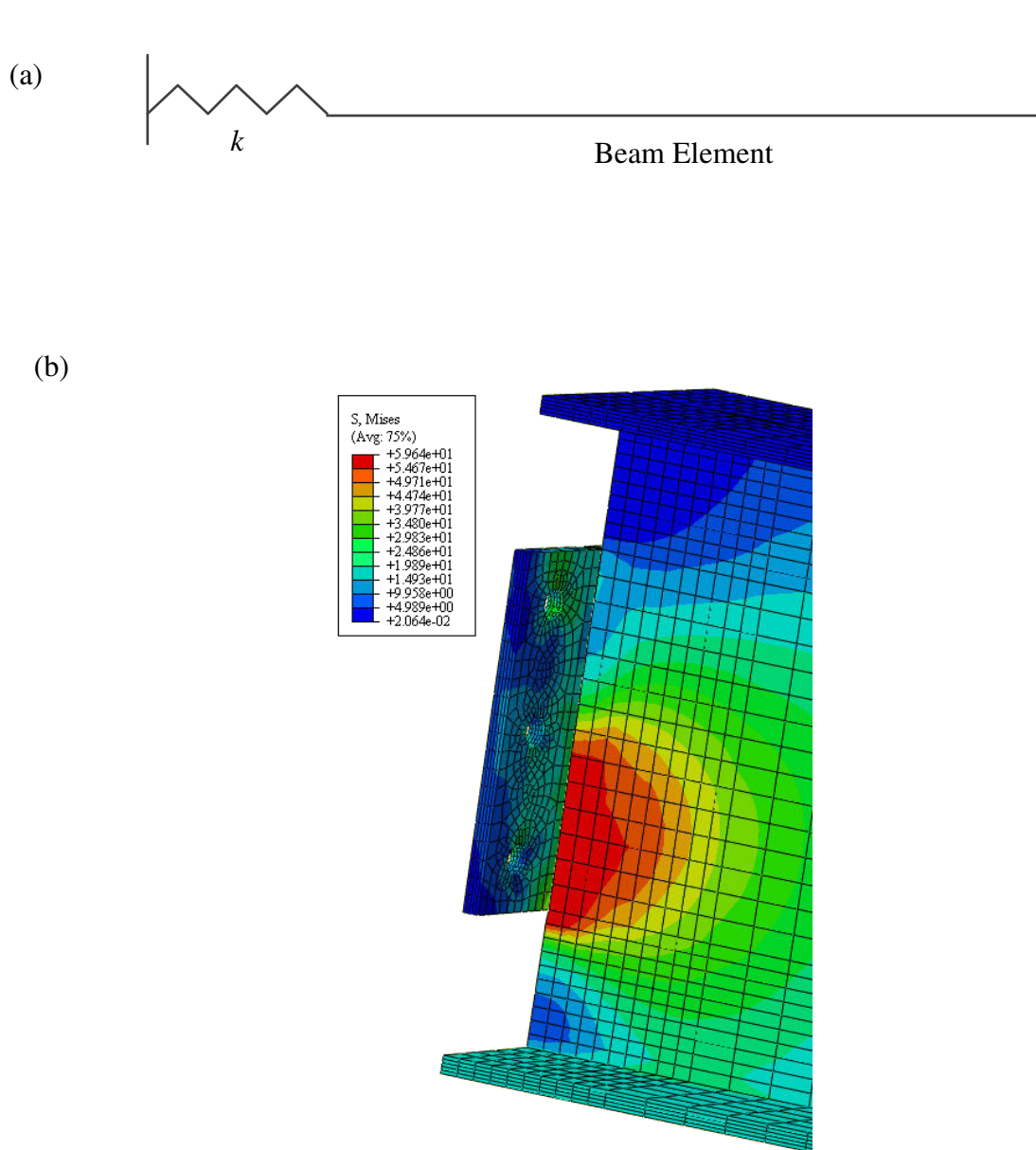


Fig. 19. (a) Model of beam, connection and column as used in the mechanistic model, (b) von Mises stress contour in the beam at the beginning of the heating stage (sI)

Direct stiffness method is used to determine the thermally induced axial force in the beam and connection element. The beam element stiffness matrix, K_b , is:

$$K_b = \begin{bmatrix} \frac{E_b A_b}{L_b} & 0 & 0 & -\frac{E_b A_b}{L_b} & 0 & 0 \\ 0 & \frac{12E_b I_b}{L_b^3} & \frac{6E_b I_b}{L_b^2} & 0 & -\frac{12E_b I_b}{L_b^3} & \frac{6E_b I_b}{L_b^2} \\ 0 & \frac{6E_b I_b}{L_b^2} & \frac{4E_b I_b}{L_b} & 0 & -\frac{6E_b I_b}{L_b^2} & \frac{2E_b I_b}{L_b} \\ -\frac{E_b A_b}{L_b} & 0 & 0 & \frac{E_b A_b}{L_b} & 0 & 0 \\ 0 & -\frac{12E_b I_b}{L_b^3} & -\frac{6E_b I_b}{L_b^2} & 0 & \frac{12E_b I_b}{L_b^3} & -\frac{6E_b I_b}{L_b^2} \\ 0 & \frac{6E_b I_b}{L_b^2} & \frac{2E_b I_b}{L_b} & 0 & -\frac{6E_b I_b}{L_b^2} & \frac{4E_b I_b}{L_b} \end{bmatrix}$$

where E_b is the modulus of elasticity of the beam, I_b is the moment of inertia, L_b is the length of the beam, and A_b is the cross sectional area of the beam.

The spring element stiffness matrix, K_s , is given as:

$$K_s = \begin{bmatrix} k & -k \\ -k & k \end{bmatrix}$$

where k corresponds to the elastic or plastic stiffness of the spring element, and can be computed according to Al-Jabri et al. [6]:

$$k = \begin{cases} \frac{E_c t_{cw} b_{effcw}}{d_{cw}} & \text{for the elastic state} \\ \frac{E_{Tc} t_{cw} b_{effcw}}{d_{cw}} & \text{for the plastic state} \end{cases} \quad (1)$$

where E_c is the modulus of elasticity of the column, E_{Tc} is the tangent modulus of elasticity of the column, t_{cw} is the thickness of the column web; b_{effcw} is the effective width of the column web, assumed equal to the depth of the endplate plus five times the distance from the outer face flange to the web toe fillet; and d_{cw} is the depth of the column web between fillets.

The global matrix, K , can be written as follows:

$$K = \begin{bmatrix} \frac{E_b A_b}{L_b} & 0 & 0 & -\frac{E_b A_b}{L_b} & 0 & 0 \\ 0 & \frac{12E_b I_b}{L_b^3} & \frac{6E_b I_b}{L_b^2} & 0 & -\frac{12E_b I_b}{L_b^3} & \frac{6E_b I_b}{L_b^2} \\ 0 & \frac{6E_b I_b}{L_b^2} & \frac{4E_b I_b}{L_b} & 0 & -\frac{6E_b I_b}{L_b^2} & \frac{2E_b I_b}{L_b} \\ -\frac{E_b A_b}{L_b} & 0 & 0 & \frac{E_b A_b}{L_b} + k & 0 & 0 \\ 0 & -\frac{12E_b I_b}{L_b^3} & -\frac{6E_b I_b}{L_b^2} & 0 & \frac{12E_b I_b}{L_b^3} & -\frac{6E_b I_b}{L_b^2} \\ 0 & \frac{6E_b I_b}{L_b^2} & \frac{2E_b I_b}{L_b} & 0 & -\frac{6E_b I_b}{L_b^2} & \frac{4E_b I_b}{L_b} \end{bmatrix}$$

The structure stiffness equation becomes:

$$\begin{bmatrix} \frac{E_b A_b}{L_b} & 0 & 0 & -\frac{E_b A_b}{L_b} & 0 & 0 \\ 0 & \frac{12E_b I_b}{L_b^3} & \frac{6E_b I_b}{L_b^2} & 0 & -\frac{12E_b I_b}{L_b^3} & \frac{6E_b I_b}{L_b^2} \\ 0 & \frac{6E_b I_b}{L_b^2} & \frac{4E_b I_b}{L_b} & 0 & -\frac{6E_b I_b}{L_b^2} & \frac{2E_b I_b}{L_b} \\ -\frac{E_b A_b}{L_b} & 0 & 0 & \frac{E_b A_b}{L_b} + k & 0 & 0 \\ 0 & -\frac{12E_b I_b}{L_b^3} & -\frac{6E_b I_b}{L_b^2} & 0 & \frac{12E_b I_b}{L_b^3} & -\frac{6E_b I_b}{L_b^2} \\ 0 & \frac{6E_b I_b}{L_b^2} & \frac{2E_b I_b}{L_b} & 0 & -\frac{6E_b I_b}{L_b^2} & \frac{4E_b I_b}{L_b} \end{bmatrix} \Delta = P + \text{Fixed End Forces}$$

where Δ corresponds to the vector of nodal displacements, P corresponds to the vector of external applied forces at the nodes, and the *fixed end forces* correspond to the vector of forces induced by change in temperature.

Solving the above system gives:

$$\Delta = \frac{E_b A_b \alpha \Delta T}{\left(\frac{E_b A_b}{L_b} + k \right)} \quad (2)$$

where α is defined as the coefficient of thermal expansion, and ΔT corresponds to the temperature increment.

The internal axial force in the beam, P , can be obtained as follows:

$$P = k\Delta = \frac{kE_b A_b \alpha \Delta T}{\left(\frac{E_b A_b}{L_b} + k \right)} \quad (3)$$

It should be noted that the spring stiffness k , modulus of elasticity E , and coefficient of thermal expansion α , vary with temperature. The internal axial force at a certain temperature, $T_{(i)}$, can be written as follows:

$$P_{(i)} = k_{(i)}\Delta = \frac{k_{(i)}E_{b(i)} A_b \alpha_{(i)} \Delta T}{\left(\frac{E_{b(i)} A_b}{L_b} + k_{(i)} \right)} \quad (4)$$

C. Formulation of the Response for Proposed Model I

The axial force developed in the beam is mainly due to the resistance of the beam, endplate, and column web as the axial force is transferred from the beam through the connection to the column.

1. Mechanism in (sI)

During the first stage of the heating phase of a fire (sI), the compressive axial force in the beam is mainly due to the endplate restraining the expansion of the beam web as shown in Fig. 19(b). The axial force at each temperature increment, ΔT , can be written as follows:

$$P_{(i)} = k_{(i)}\Delta = \frac{k_{(i)}E_{b(i)} A_{bw} \alpha_{(i)} (T_{(i)} - 20)}{\left(\frac{E_{b(i)} A_{bw}}{L_b} + k_{(i)} \right)} \quad (5)$$

where A_{bw} is the area of the beam web.

As the temperature increases, the axial force developed in the beam increases and two limit states might occur: either column web buckling, or elastic beam web buckling. The force that causes buckling in the column at elevated temperature, $P_{cwcw(i)}$, and the effective buckling width of the column web, b_{eff-c} , can be written as follows, respectively [25]:

$$P_{cwcw(i)} = 8.4b_{eff-c}^{0.017}d_c^{0.96}t_{cw}^{1.43}f_{ycw(i)}^{0.76} \quad (6)$$

$$b_{eff-c} = t_{bf} + 2\sqrt{2}a_p + 5(t_{cf} + r_c) \quad (7)$$

where d_c is the depth of the column, $f_{ycw(i)}$ is the column web yield strength at a given temperature, t_{bf} is the thickness of the beam flange, a_p is the size of the fillet weld, t_{cf} is the thickness of the column flange, and r_c is the root radius of the column.

A modified expression for computing the beam web critical buckling load is used based on Usmani et al. [26]:

$$P_{crbw(i)} = \frac{\pi^2 E_{b(i)} I_b}{L_b^2} \times \left(\frac{A_{bw}}{A_b} \right)^2 \quad (8)$$

At each temperature increment, the axial force $P_{(i)}$ is calculated and compared to $P_{cwcw(i)}$ (Eq.(6)) and $P_{crbw(i)}$ (Eq.(8)). The incremental procedure continues until one of the two limit states is reached. Beam web buckling governed in all the cases studied.

2. Mechanism in (s2)

When local buckling of the beam web occurs, only part of the beam web area is considered in computing the axial force. To compute the axial force, the reduced beam web area, A_{bwr} , needs to be calculated.

First, the reduced beam web area is calculated at each temperature increment, ΔT , as follows:

The temperature at each increment is computed using the following equation:

$$T_{(i)} = T_{(i-1)} + \Delta T \quad (9)$$

where $T_{(i)}$ is the temperature at the current step, $T_{(i-1)}$ is the temperature at the previous step, and ΔT is the temperature increment.

The beam web area at any given temperature, $T_{(i)}$, can be written as follows:

$$A_{bwr(i)} = A_{bwr(i-1)} + \Delta A_{bwr} \quad (10)$$

where $A_{bwr(i)}$ is the beam web area at the current step, $A_{bwr(i-1)}$ is the beam web area at the previous step, and ΔA_{bwr} is the beam web area increment.

The axial load at any given temperature, $T_{(i)}$, is given as:

$$P_{(i)} = P_{(i-1)} + \Delta P \quad (11)$$

where $P_{(i)}$ is the axial force at the current step, $P_{(i-1)}$ is the axial force at the previous step, and ΔP is the axial force increment.

The beam web area at any given temperature, $A_{bwr(i)}$, can be written as a linear relationship:

$$\frac{A_{bwr(i)}}{A_{bw}} = a_1 \left(\frac{P_{(i-1)}}{P_{crbw}} \right) + b_1 \quad (12)$$

where P_{crbw} is the axial force at the end of (sI), a_1 and b_1 are constants, and their values are tabulated in Table 3. Note that a_1 and b_1 are dependent on the following parameters: load ratio, beam length, and endplate thickness, and the computation of a_1 and b_1 is presented below. a_1 and b_1 are computed by conducting a parametric study that covers most possible cases associated with W16x36 beam. Load ratios of (0.25, 0.33, 0.5), endplate thicknesses of (0.375, 0.5, 0.6, 0.7 in), and beam lengths of (20, 25, 30, 35, 40,

45 ft) are considered in computing a_1 and b_1 . It was found from the FE results that the axial compressive force decreases due to the reduced beam web area at each temperature increment. This is due to the post-buckling effect of the beam web.

The ratio of the reduced beam web area (from the FE) to the total beam web area, ($A_{bwr(i)}/A_{bw}$), is plotted against the ratio of the axial force (from the FE analysis) to the critical beam web buckling load, ($P_{(i-1)}/P_{crbw}$), as shown in Fig. 20. The data points for each case are found to capture a linear fit with an acceptable coefficient of determination. The values of the slope (a_1) and y-intercept (b_1) for each case are presented in Table 3.

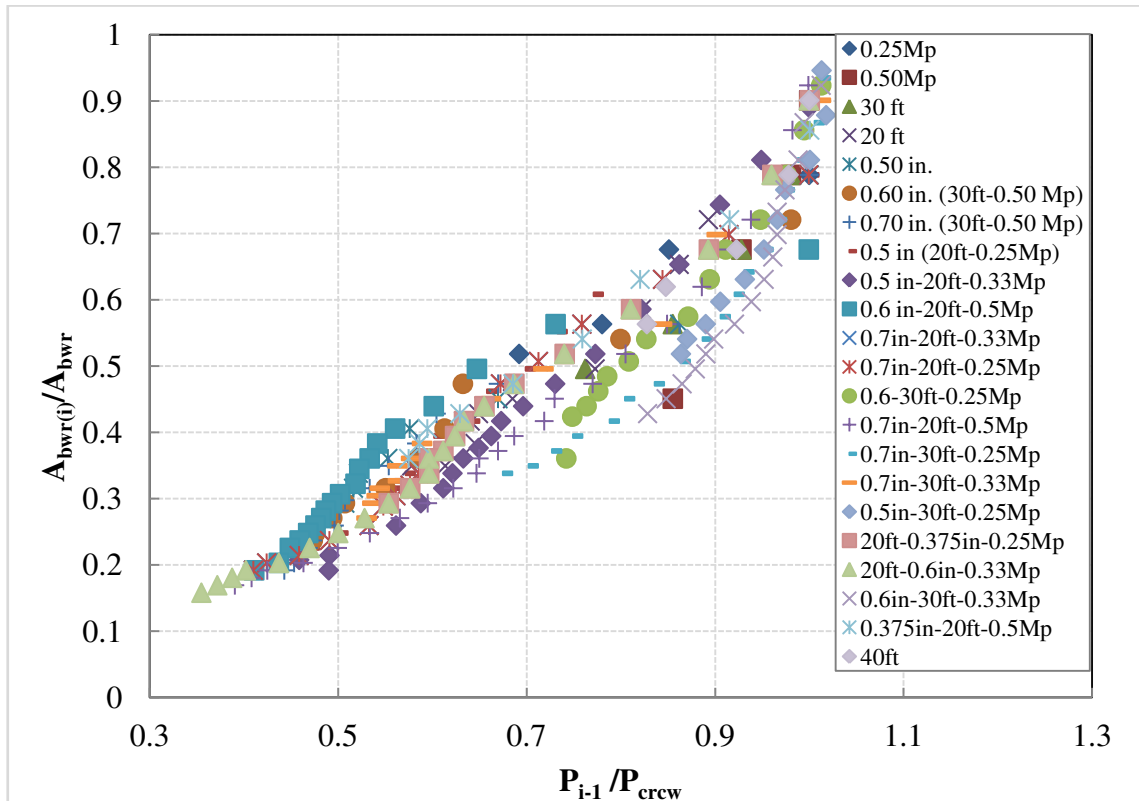


Fig. 20. The reduction in the area of the beam web at the current step (i) as a function of the axial force at the previous step ($i-1$)

Table 3. Buckling and contact parameters for different load ratios, beam lengths, and endplate thickness

Column Section	Beam Section	Case	Beam Length (ft)	Endplate Thickness (in)	Endplate Location ¹ (in)	LR ²	a ₁	b ₁	a ₂	b ₂
W14x90	W16x36	1	20	0.375	+0.00	0.5	1.095	-0.266	0.323	-
		2	20	0.375	+0.00	0.33	1.256	-0.412	0.405	-
		3	20	0.375	+0.00	0.25	1.234	-0.385	0.455	-
		4	20	0.5	+0.00	0.5	1.278	-0.438	0.555	-
		5	20	0.5	+0.00	0.33	1.305	-0.459	0.740	-
		6	20	0.5	+0.00	0.25	1.122	-0.294	0.612	-
		7	20	0.6	+0.00	0.5	0.909	-0.152	0.496	-
		8	20	0.6	+0.00	0.33	1.092	-0.279	0.699	-
		9	20	0.6	+0.00	0.25	1.091	-0.277	0.795	-
		10	20	0.7	+0.00	0.5	1.141	-0.354	0.766	-
		11	20	0.7	+0.00	0.33	1.076	-0.280	0.709	-
		12	20	0.7	+0.00	0.25	1.077	-0.280	1.075	-
		13	25	0.375	+0.00	0.5	1.038	-0.118	0.492	-
		14	30	0.375	+0.00	0.5	2.946	-2.068	0.221	-
		15	30	0.375	+0.00	0.33	1.604	-0.768	0.330	-
		16	30	0.375	+0.00	0.25	0.917	-0.125	0.290	-
		17	30	0.5	+0.00	0.5	0.897	-0.147	0.352	-
		18	30	0.5	+0.00	0.33	2.432	-1.708	0.265	-
		19	30	0.5	+0.00	0.25	1.784	-0.937	0.418	-
		20	30	0.6	+0.00	0.5	1.071	-0.258	0.332	-
		21	30	0.6	+0.00	0.33	2.622	-1.805	0.378	-
		22	30	0.6	+0.00	0.25	1.783	-0.937	0.505	-
		23	30	0.7	+0.00	0.5	0.999	-0.227	0.343	-
		24	30	0.7	+0.00	0.33	1.132	-0.308	0.516	-
		25	30	0.7	+0.00	0.25	0.163	-0.836	0.511	-
		26	35	0.375	+0.00	0.5	1.226	-0.226	0.296	-
		27	45	0.375	+0.00	0.5	1.093	0.061	0.143	-
		28	30	0.375	+0.00	0.85	-0.41	1.364	1.913	-
		29	30	0.375	+0.00	0.9	-0.76	1.711	3.593	-
		30	30	0.375	+0.00	0.92	-0.43	1.408	1.524	-
		31	30	0.375	+0.00	1	-1.25	2.115	0.992	-
		32	30	0.375	+1.27	0.5	2.946	-2.068	0.221	-

¹The location of the endplate (in.) is tabulated with respect to the neutral axis (N.A) (positive sign=above N.A, negative sign=below N.A)

²LR: load ratio

The axial force, $P_{(i)}$, at any given temperature, $T_{(i)}$, can be written as:

$$P_{(i)} = k_{(i)} \Delta = \frac{k_{(i)} E_{b(i)} A_{bwr(i)} \alpha_{(i)} (T_{(i)} - 20^\circ\text{C})}{\left(\frac{E_{b(i)} A_{bwr(i)}}{L_b} + k_{(i)} \right)} \quad (13)$$

The design engineer uses the values of a_l and b_l presented in Table 3 to calculate the critical buckling load, P_{crbw} , and the beam web area, $A_{bwr(0)}$, at the onset of buckling, which is the full area of the beam web, A_{bw} , then computes the reduced area for the first temperature increment after the onset of buckling, $A_{bwr(1)}$, and its corresponding axial force, $P_{(1)}$. This axial force, $P_{(1)}$, is used to calculate the reduced beam web area for the second temperature increment, $A_{bwr(2)}$. This incremental procedure continues until beam flange contact occurs. Contact is determined by checking the beam end rotation at each temperature increment. The beam end rotation at the onset of contact is equal to the geometric angle of contact between the bottom beam flange and the column, θ_c , shown in Fig. 21.

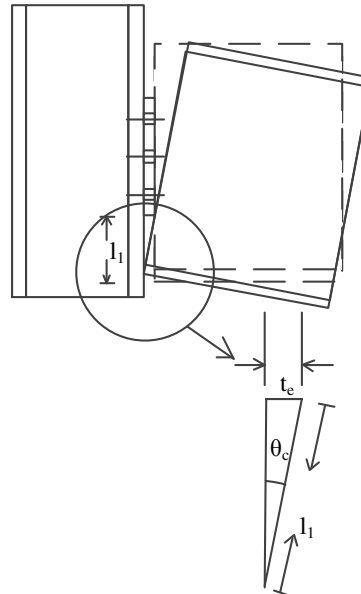


Fig. 21. Contact between the lower beam flange and the column

θ_c can be written as follows:

$$\theta_c = \frac{t_e}{l_1} \quad (14)$$

where t_e is the shear endplate thickness, and l_1 is the distance from the edge of the endplate to the external side of the lower flange of the beam as shown in Fig. 21.

The beam end rotation, $\theta_{(i)}$, for a simply supported beam in the elastic range, at any given temperature, $T_{(i)}$, is given by Selamet and Garlock [16]. A modification factor $p_{(i)}$ was added to the equation in order to reduce the moment of inertia of the beam, I_b , since part and not all the beam section is contributing to the force.

$$\theta_{(i)} = \frac{w \times L_b^3 \times p_{(i)}}{8 \times E_{b(i)} \times I_b} \quad (15)$$

where w is the applied load on the beam, and $p_{(i)} = \frac{A_b}{A_{bwr(i)}}$

3. Mechanism in (s3)

After contact, the lower beam flange is subjected to compression loading. The total axial load is now composed of two parts which come from the contribution of the beam web and the beam flange [16]. In this case, the total area of the beam section that is working in compression can be written as follows:

$$A_{bc(i)} = A_{bwr} + A_{bfc(i)} \quad (16)$$

where $A_{bc(i)}$ is the total beam section area contributing to the axial force, A_{bwr} is the reduced beam web area at the end of (s2), and $A_{bfc(i)}$ is the contact flange area contributing to the axial force at each temperature increment. To compute the axial

force, the flange contact area contributing to the axial force, $A_{bfc(i)}$, needs to be calculated.

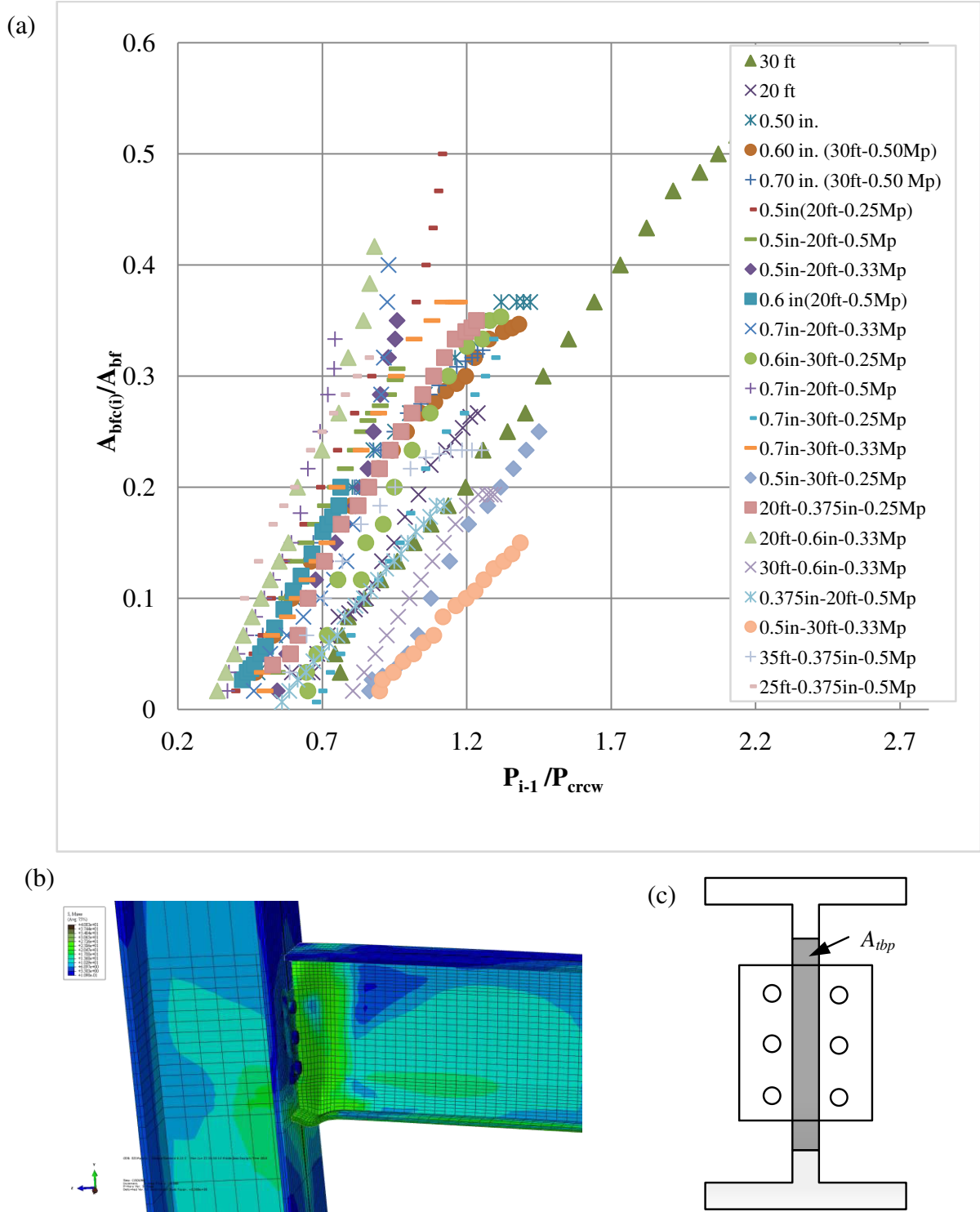


Fig. 22. (a) The increase in the flange contact area contributing to the axial as a function of the axial force at the previous step, (b) increased deflection in the beam after lower beam flange buckling, (c) tributary contact area of the beam web

First, the flange contact area is calculated at each temperature increment, ΔT , as follows:

The temperature at each increment, $T_{(i)}$, is computed using Eq.(8).

The flange contact area contributing to the axial force at any given temperature, $T_{(i)}$, can be written as follows:

$$A_{bfc(i)} = A_{bfc(i-1)} + \Delta A_{bfc} \quad (17)$$

where $A_{bfc(i)}$ is the flange contact area at the current step, $A_{bfc(i-1)}$ is the flange contact area at the previous step, and ΔA_{bfc} is the flange contact area increment.

The axial load at any given temperature is given by Eq.(10).

The flange contact area contributing to the axial force at any given temperature, $T_{(i)}$, can be expressed as a linear relationship:

$$\frac{A_{bfc(i)}}{A_{bf}} = a_2 \left(\frac{P_{(i-1)}}{P_{crbw}} \right) + b_2 \quad (18)$$

where a_2 and b_2 are constants, and their values are tabulated in Table 3. Note that a_2 and b_2 are dependent on the following parameters: load ratio, beam length, and endplate thickness, and the computation of a_2 and b_2 is similar to that of a_1 and b_1 and is presented below. a_2 and b_2 are computed from the same parametric study that was used to compute a_1 and b_1 . It was found from the FE results that the axial compressive force increases due to the lower beam flange contact area at each temperature increment.

The ratio of the flange contact area (from the FE) to the total area of the lower beam flange, $(A_{bfc(i)}/A_{bf})$, is plotted against the ratio of the axial force (from the FE analysis) to the critical beam web buckling load, $(P_{(i-1)}/P_{crbw})$ (Fig. 22(a)). The data for each case is found to capture a linear fit with an acceptable coefficient of determination. The values of the slope (a_2) and y-intercept (b_2) for each case are presented in Table 3.

The axial force, $P_{(i)}$, at any given temperature, $T_{(i)}$, can be written as follows:

$$P_{(i)} = k_{(i)} \Delta = \frac{k_{(i)} E_{b(i)} A_{bc(i)} \alpha_{(i)} (T_{(i)} - 20^\circ C)}{\left(\frac{E_{b(i)} A_{bc(i)}}{L_b} + k_{(i)} \right)} \quad (19)$$

When the area of the beam flange increases, the total compressive axial force in the beam increases with each temperature increment. This increase is limited by plastic buckling of the lower flange of the beam at temperature T_{Pmax} with a maximum axial force P_{max} and contact area $A_{bc(max)}$.

A modified expression for computing the beam lower flange critical buckling load is used based on Usmani et al. [26]:

$$P_{crbf(i)} = \frac{\pi^2 E_{b(i)} I_b}{L_b^2} \times \left(\frac{A_{fc(i)}}{A_b} \right)^2 \quad (20)$$

The contribution of the lower flange of the beam axial compressive force to the total force can be described as the difference between the total axial compressive force and the critical web buckling load:

$$P_{bfc(i)} = P_{(i)} - P_{crbw} \quad (21)$$

Lower beam flange buckling occurs when the contribution of the lower beam flange, $P_{bfc(i)}$, defined in Eq.(21) reaches the critical lower flange buckling load, $P_{crbf(i)}$, defined in Eq.(20).

4. Mechanism in (s4)

After the onset of plastic lower flange buckling (s4), the whole beam contact area contributing to the axial force starts to plastify. The maximum ratio of the plastic strain to the elastic strain, at a certain temperature, $T_{(i)}$, defined as $q_{(i)}$, can be computed

using the equation below. Note that Eq.(22) is used for a temperature greater than the temperature that causes lower beam flange buckling T_{Pmax} :

$$q_i = \begin{cases} 50 \times \sqrt{\frac{30}{500 - T_i}} & \text{for } T_{Pmax} < T_i < 470^\circ\text{C} \\ 50 & \text{for } T_i > 470^\circ\text{C} \end{cases} \quad (22)$$

After plastic buckling of the lower beam flange occurs, the tangent modulus of elasticity is used. The axial force at any given temperature $T_{(i)}$ can be expressed as the summation of the axial force at the previous step, $P_{(i-1)}$, and the axial force increment caused by the temperature increment ΔT . The axial force can be written as:

$$P_{(i)} = P_{(i-1)} + E_{Tb(i)} A_{bc(max)} \alpha_{(i)} \Delta T \times \frac{k_{(i)}}{\left(\frac{E_{Tb(i)} A_{bc(max)}}{L_b} + k_{(i)} \right)} \times q_{(i)} \quad (23)$$

where $E_{Tb(i)}$ is the tangent modulus of elasticity of the beam.

At this stage, the plastic buckling of the beam as well as the yielding of the column web and flange near the contact region causes a significant increase in the beam deflection as shown in Fig. 22(b). The significant deflection in the beam at about 500°C causes the whole beam section to act in catenary. However, due to previous buckling in the beam section, the buckled area is not taken into account. The area of the beam section working in catenary, A_{ct} , becomes:

$$A_{ct} = A_b - A_{bc(max)} \quad (24)$$

The axial force in the beam can be written as follows:

$$P_{(i)} = P_{(i-1)} + E_{Tb(i)} A_{ct} \alpha_{(i)} \Delta T \times \frac{k_{(i)}}{\left(\frac{E_{Tb(i)} A_{ct}}{L_b} + k_{(i)} \right)} \times q_{(i)} \quad (25)$$

The significant geometric deformation in the beam and connection causes tensile and bending forces to develop in the tension bolts and might lead to bolt failure. The bolt force needs to be checked at each temperature increment. It is assumed that the bolt force was increased by an amount of 15%.

At any given temperature, $T_{(i)}$, the bolt force is given by the following equation:

$$B_{f(i)} = \frac{1.15(P_{\max} - P_{(i)})}{n_{tb}} \quad (26)$$

where n_{tb} is the number of tension bolts in the connection.

The critical bolt force is given as:

$$B_{cr(i)} = f_{ub(i)} A_{tb} \quad (27)$$

where A_{tb} is the area of the bolt, and $f_{ub(i)}$ is the ultimate stress in the bolt at a given temperature $T_{(i)}$.

The connection fails when the bolt force $B_{f(i)}$ defined in Eq.(26) reaches the critical bolt force $B_{cr(i)}$ defined in Eq.(27).

D. Formulation of the Response for Proposed Model II

The axial force developed in the beam for type II mechanism is mainly due to the resistance of the beam, endplate, and column web as the axial force is transferred from the beam through the connection to the column.

1. Mechanism in (s1)

The axial force in the beam for type II mechanism in the first stage of the heating phase (s1) is given by Eq.(5).

As the temperature increases, the axial force developed in the beam increases and three limit states can occur: (1) column web buckling, (2) local elastic beam web buckling, and (3) beam web yielding. The force that causes buckling in the column is given in Eq.(6).

The load ratio in mechanism type II is large (> 0.85). The beam develops large stresses prior to heating. These stresses lead to a reduction in the critical beam web buckling load $P_{crbw(i)}$ accounted for in Eq.(7). The connection is considered a pinned joint. Thus, 25% of the applied moment is transferred from the beam to the connection. The critical beam web buckling load can be written as follows:

$$P_{crbw(i)} = \frac{\pi^2 E_{b(i)} I_b}{L_b^2} \times \left(\frac{A_{bw}}{A_b} \right)^2 - \frac{0.25M}{d_p} \quad (28)$$

where d_p corresponds to the depth of the endplate, and M corresponds to the applied moment on the beam at ambient temperature.

The load that causes yielding of the beam web can be written as follows:

$$P_{bwy(i)} = f_{by(i)} A_{tbp} - \frac{0.25M}{d_p} \quad (29)$$

where $f_{by(i)}$ corresponds to the yield stress in the beam, A_{tbp} corresponds to the tributary area of the beam web in the vicinity of the plate as shown in Fig. 22(c).

For each temperature increment, the axial force $P_{(i)}$ (Eq.(5)) is compared to the limit states loads (Eq.(6)), Eq.(28), and Eq.(29)). The incremental procedure continues until any of the limit states is reached. Although the three limit states were checked for the models, local buckling in the beam web occurred followed by beam web yielding.

2. Mechanism in (s2)

When local buckling of the beam web occurs, the area of the beam contribution to the axial force is reduced (similar to mechanism type I). The reduced area of the beam web is determined using Eq.(12), where the values of a_I and b_I are presented in Table 3.

The total axial force in the beam is given by Eq.(13). The reduction in the area of the beam web continues until yielding of the beam web occurs. This occurs when the axial force, $P_{(i)}$, given by Eq.(13) reaches the beam web yielding load, $P_{bwy(i)}$, given by Eq.(29).

3. Mechanism in (s3)

After yielding of the beam web occurs, the elastic modulus of elasticity is substituted by the tangent modulus of elasticity, $E_{Tb(i)}$. The axial force, P_i , can be written as follows:

$$P_{(i)} = P_{(i-1)} + \frac{k_{(i)} E_{Tb(i)} A_{bwr} \alpha_{(i)} \Delta T}{\left(\frac{E_{Tb(i)} A_{bwr}}{L_b} + k_{(i)} \right)} \quad (30)$$

where A_{bwr} is the minimum reduced area obtained in (s2).

The incremental procedure continues until contact occurs between the lower beam flange and the column, when the beam end rotation reaches the geometric contact angle computed by Eq.(14) and shown in Fig. 20(b).

The beam end rotation for a simply supported beam in the plastic range is given by Selamet and Garlock [16] in the following equation:

$$\theta_{(i)} = \frac{w \times L_b^3 \times p_{(i)}}{24 \times E_{b(i)} \times I_b} \quad (31)$$

4. Mechanism in (s4)

After contact, the lower beam flange is also loaded in compression. The total area of the beam section is given in Eq.(16). Note that the lower beam flange contact area is in the elastic state while the beam web area is in the plastic state. The flange contact area is calculated by Eq.(18) where a_2 and b_2 are presented in Table 3.

The internal axial force in the beam can be written as follows:

$$P_{(i)} = k_{(i)}\Delta = \frac{k_{(i)}E_{Tb(i)}A_{bwr}\alpha_{(i)}\Delta T}{\left(\frac{E_{Tb(i)}A_{bwr}}{L_b} + k_{(i)}\right)} + \frac{k_{(i)}E_{b(i)}A_{bfc(i)}\alpha_{(i)}\Delta T}{\left(\frac{E_{b(i)}A_{bfc(i)}}{L_b} + k_{(i)}\right)} \quad (32)$$

The axial compressive force increases again and is limited by local lower flange buckling followed by yielding of the lower flange. The load that causes local buckling in the lower flange of the beam is given by the following formula:

$$P_{crbf(i)} = \frac{\pi^2 E_{b(i)} I_b}{L_b^2} \times \left(\frac{A_{bfc(i)}}{A_b}\right)^2 - \frac{0.25M}{d_p + l_1} \quad (33)$$

5. Mechanism in (s5)

After local buckling occurs in the lower beam flange, the flange contact area is reduced similar to the beam web reduction in (s2). The axial force in the beam can be written as follows:

$$P_{(i)} = k_{(i)}\Delta = \frac{k_{(i)}E_{T(i)}A_{bwr}\alpha_{(i)}\Delta T}{\left(\frac{E_{T(i)}A_{bwr}}{L_b} + k_{(i)}\right)} + \frac{k_{(i)}E_{b(i)}A_{bfr(i)}\alpha_{(i)}\Delta T}{\left(\frac{E_{b(i)}A_{bfr(i)}}{L_b} + k_{(i)}\right)} \quad (34)$$

where $A_{bfr(i)}$ corresponds to the reduced lower beam flange contact area (current step).

The incremental procedure continues until lower beam flange yielding occurs. The load that causes lower beam flange yielding is given by the following equation:

$$P_{bfy(i)} = f_{by(i)} A_{bfr(i)} - \frac{0.25M}{d_p + l_1} \quad (35)$$

6. Mechanism in (s6)

After buckling of the lower beam flange occurs, followed by lower beam flange yielding, the axial force is given by Eq.(23) and Eq.(25) depending on the temperature (below or above 500 °C respectively). The bolts fail when the bolt force given in Eq.(26) reaches the critical bolt force given in Eq.(27).

Mechanistic Models vs. FE Results

The stiffness terms are derived to be applied in an incremental computer automated iterative solution as shown in Fig. 22. The two proposed models are summarized in the flowchart, as shown in Fig. 22. Note that only the limit states that actually occurred in the connections are included in the flowchart. That is, the limit states that did not occur were not checked in the flowchart.

Figs. 23 and 24 show a comparison of the mechanistic model with the FE results for different cases (14, 32, 17, 16, 31, 30) defined in Table 3. It can be seen that the proposed model predicts the axial force in the beam with excellent agreement for all the cases. It also predicts the tension bolt failure which occurs in the heating stage.

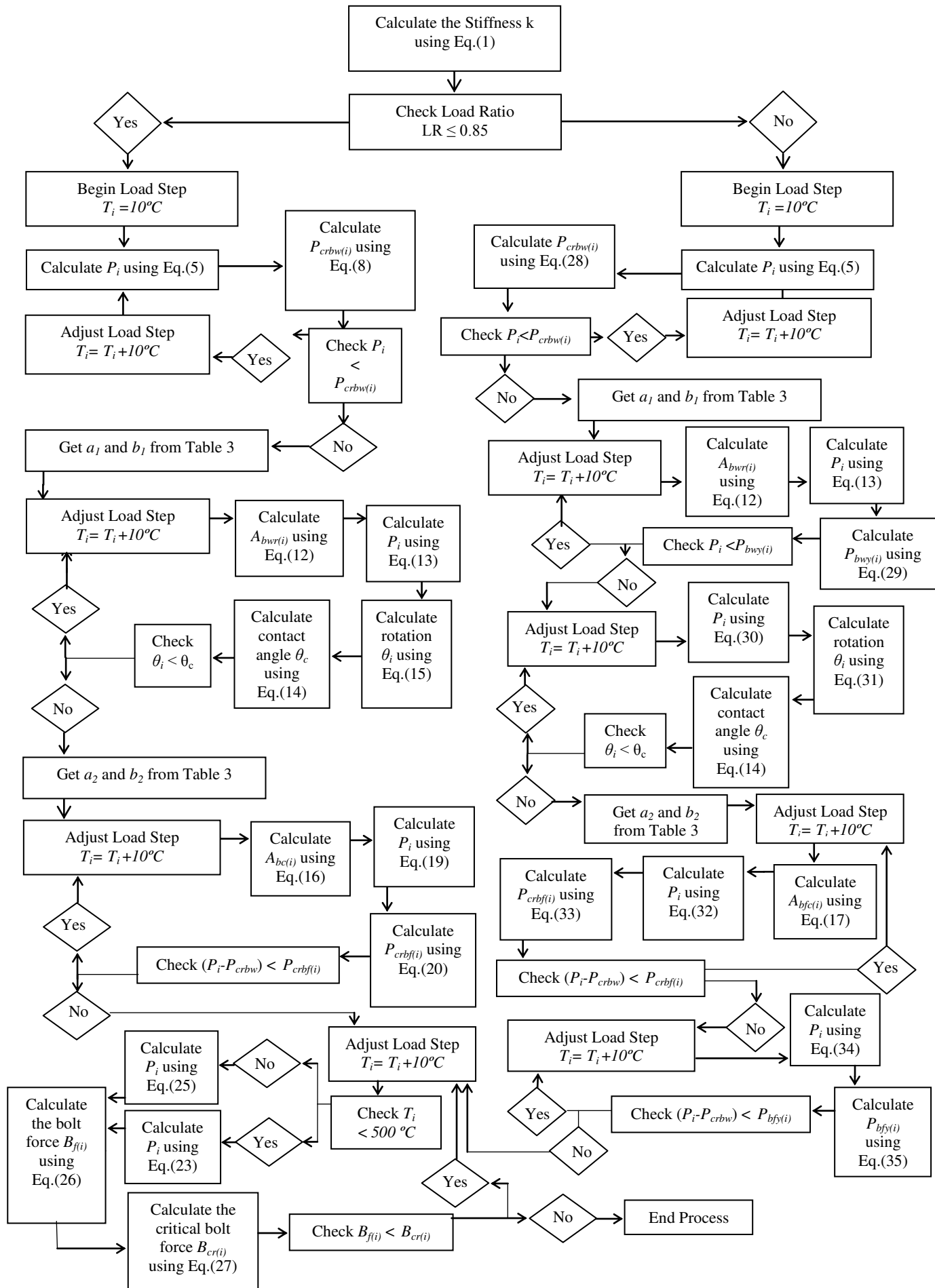


Fig. 23. Flowchart of the incremental stiffness shear endplate model

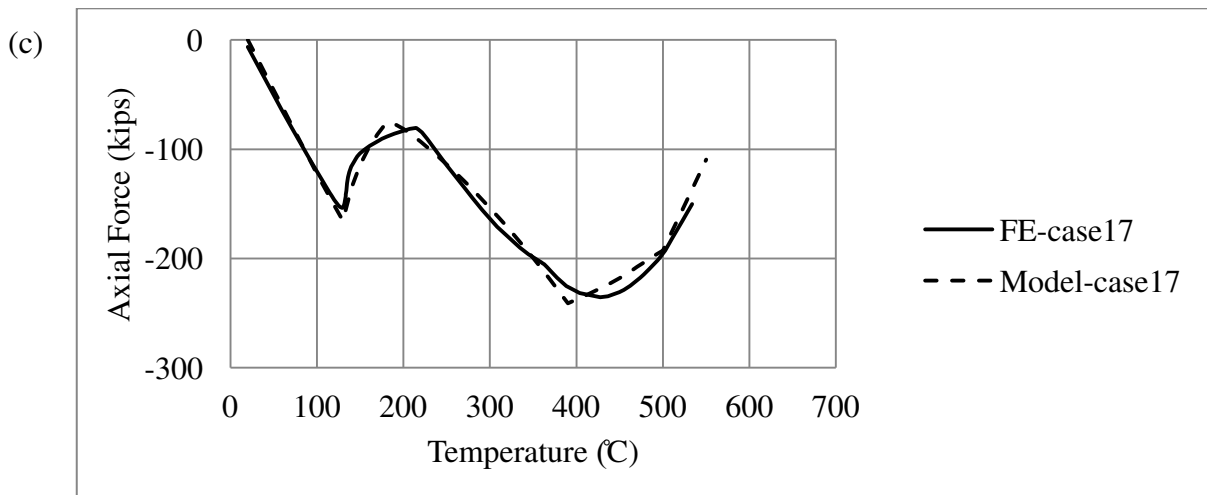
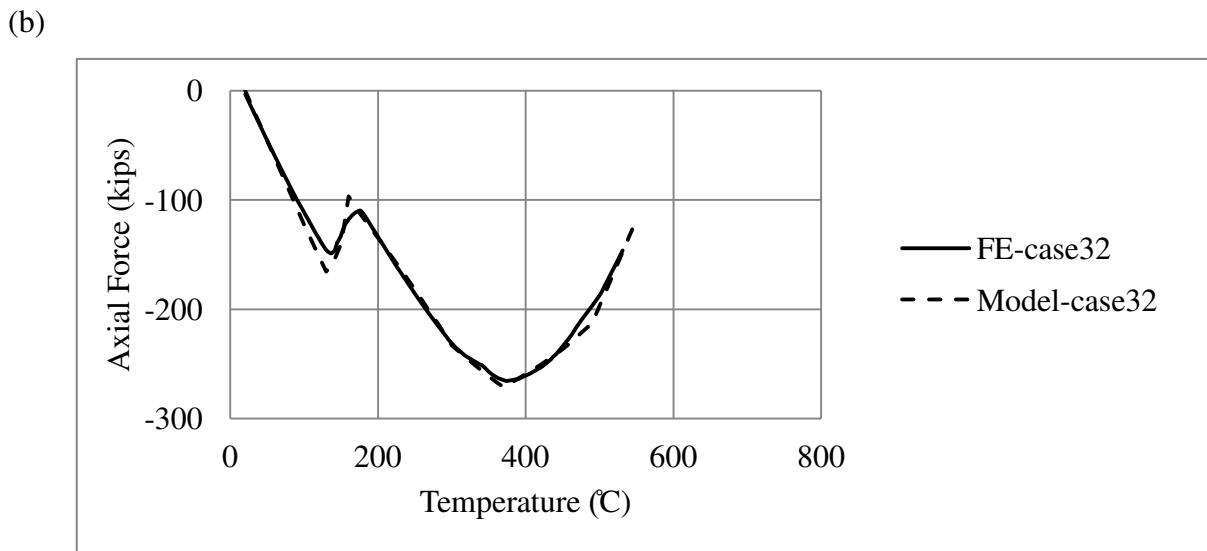
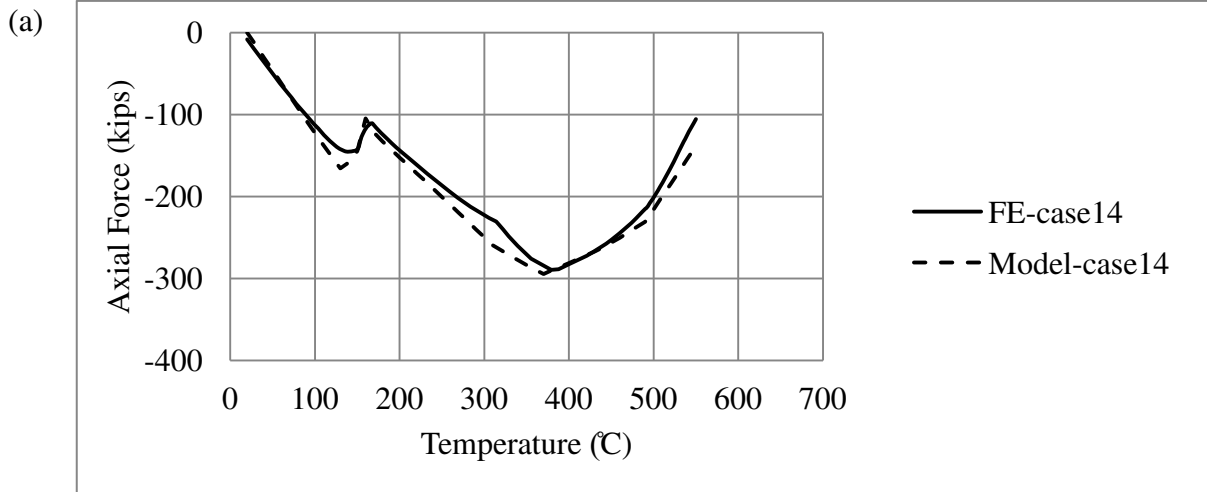


Fig. 24. Comparison of the FE results with the proposed model for different cases: (a) case 14, (b) case 32, (c) case 17

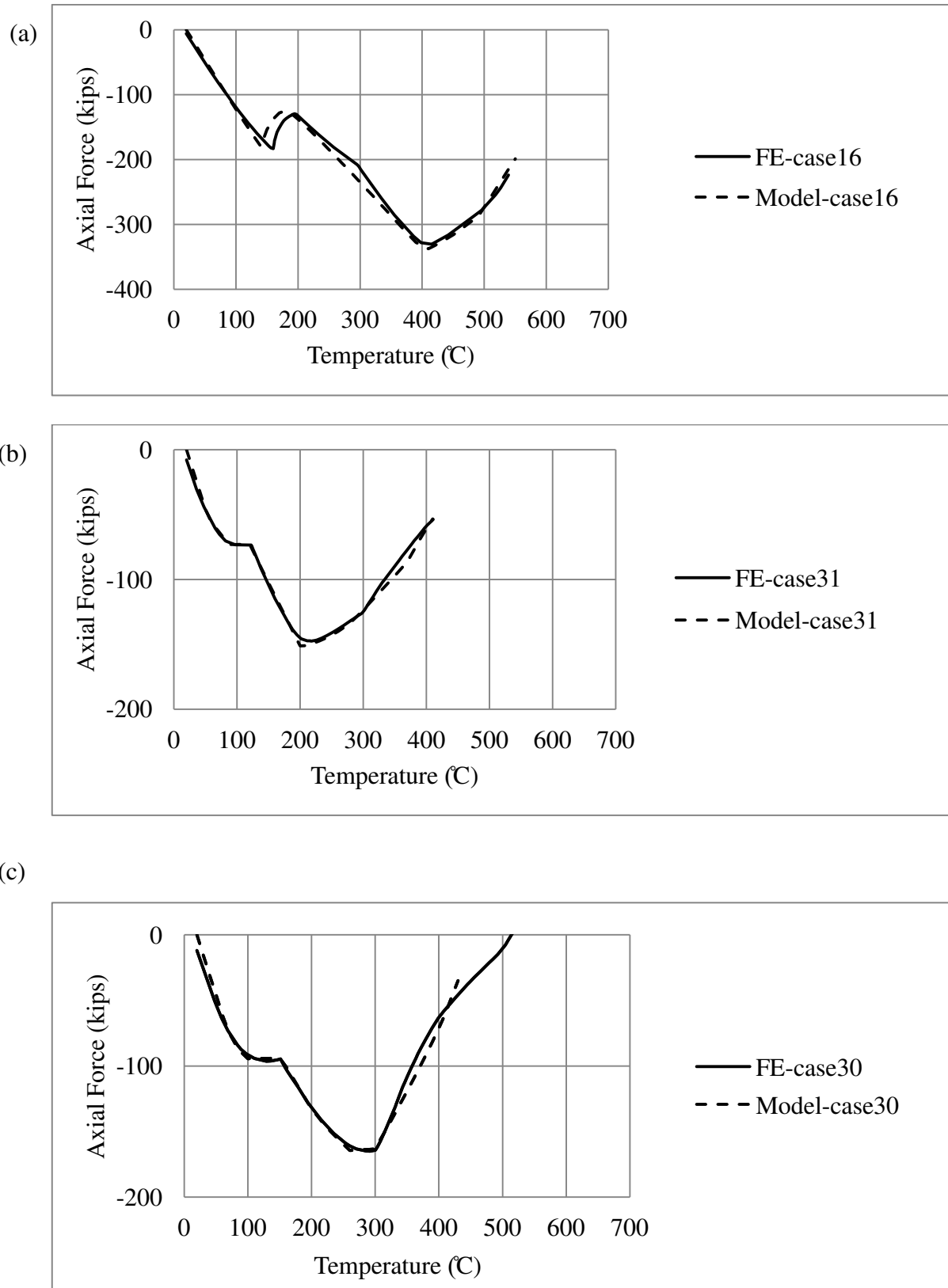


Fig. 25. Comparison of the FE results with the proposed model for different cases: (a) case 16, (b) case 31, (c) case 30

CHAPTER VI

CONCLUSIONS

Key results of a computational study on the behavior of shear endplate connections in a fire were presented in this study. An FE model of a shear endplate connection was developed and evaluated using data from elevated temperature tests conducted at the University of Sheffield [20]. FE models for connection assemblies were then used to investigate the effect of key geometric and material parameters on the behavior of shear endplate connections during a fire. A mechanistic model that predicts the force-temperature response and quantifies the thermal-induced axial forces and deformations was developed for the connection assembly. Design guidelines that quantify the fire induced thermal loads are also provided. The following conclusions are made from this research:

- FE models predict with reasonable accuracy the load-deformation response and strength of the shear endplate connection at ambient and elevated temperature. The models can also be used to predict the failure mode which was plate rupture at the toe of the weld that controls the peak strength of the connection. However, fracture modeling was not included in the simulation. Consequently, the model was not capable of predicting connection behavior after first component fracture.
- Parametric studies were conducted on a beam connected at each end to columns using shear endplate connections. These studies showed that connection response in fire is dominated by the development of very large axial forces in the beam. Very large compressive axial forces develop during the heating stage

of a fire. Shear endplate connections are therefore vulnerable to failure during the heating stage of a fire.

- During the heating stage, very large axial compressive forces are developed in the beam and beam end connections due to thermal expansion of the beam. The largest axial compressive forces are developed in the heating stage, at temperatures of about 300°C to 400°C. The results of these simulations therefore suggest that very large axial compressive forces would be expected at beam end connections for structures that have been provided insulation in accordance with U.S. building standards. That is, structures in full compliance with U.S. standards for structural-fire resistance may be vulnerable to failure at beam end connections. Note that current U.S. building standards for structural fire resistance do not explicitly consider beam-to-column connections.
- The parametric study performed on shear endplate connections shows that among the factors evaluated in this study, the main ones that impact the axial force demand on the shear endplate connection are: load ratio, beam length, and endplate thickness.
- This study shows that the load ratio on the beam at the beginning of a fire can have a significant impact on the maximum axial compressive forces that develop on the connection during a fire. FE results also indicate that increasing the beam length and endplate thickness reduce the axial compression forces developed on the connection.
- The shear endplate connections evaluated in this parametric study were only designed for gravity loads, as is typical in design practice. That is, the large axial forces expected at the connections during a fire event were not considered

in the connection design. The simulations suggest that most of the connections considered in these parametric studies would likely fail in the heating stage of a fire. The governing failure mode is tension bolt failure. This further suggests that the design procedure of the shear endplate should be modified to account for fire loading.

- The axial force demand on the shear endplate connection during a fire is higher when compared to that of the double angle and shear tab connections. The tension bolts are more vulnerable to failure when compared to the shear bolts in the double angle and shear tab connections due to the large axial force. Moreover, the shear bolts in the shear tab connection are more vulnerable to failure when compared to the shear bolts of the double angle connection because the axial force is transferred from the beam to the connection through one shear plane compared to two shear planes for the double angle connection. The failure mode encountered in the shear endplate connection during a fire is tension bolt failure.
- The FE results of the parametric study show that the load ratio impacts the global behavior of the connection during a fire. When the load ratio is greater than 0.85, the limit states encountered in the connection are: (1) local beam web buckling, (2) beam web yielding, (3) local lower flange buckling, (4) lower flange yielding, (5) tension bolt failure (failure mode). When the load ratio is less than 0.85, the limit states encountered in the connection are: (1) beam web buckling, (2) lower flange buckling, (3) tension bolt failure (failure mode).
- Based on the results of the FE simulations and experimental results, a mechanistic model was developed for the connection. The model was capable

of predicting the thermal induced forces in the beam and connection as well as the deformation and failure modes. The FE results were compared to the results of the proposed model, and the results were in excellent agreement.

Finally, it should be emphasized that the study reported in this study has several limitations. The simulations did not include: (1) the influence of the concrete slab, (2) analysis of connection performance after first component fracture, and (3) the temperature-history dependence of the bolt material. Further research is needed to evaluate these factors influence connection performance in fire.

BIBLIOGRAPHY

- [1] Ramli-Sulong N, Elghazouli A, Izzuddin B. Behaviour and design of beam-to-column connections under fire conditions. *Fire Saf J* 2007, 42(6-7): 437-451.
- [2] Bailey C, Burgess I, and Plank R. Analyses of the effects of cooling and fire spread on steel-framed buildings. *Fire Saf J* 1996, 26(4): 273-293.
- [3] Al-Jabri K. The behavior of steel and composite beam-to-column connections in fire. PhD dissertation, University of Sheffield, 1991.
- [4] Al-Jabri K. Component-based model of the behavior of flexible end-plate connections at elevated temperatures. *Composite Struct* 2004, 66(1-4): 215-221.
- [5] Al-Jabri K, Burgess I, and Plank R. Moment-rotation-temperature curves for semi-rigid joints. *J Constr Steel Res* 2005a, 61(3): 281-303.
- [6] Al-Jabri K, Burgess I, and Plank R. Spring-stiffness model for flexible end-plate bare-steel joints in fire. *J Constr Steel Res* 2005b, 61(12): 1672-1691.
- [7] Hu Y, Davidson B, Burgess I, and Plank R. Experimental Study on Flexible End Plate Connections in Fire. *Eurosteel 2008: 5th European Conference on Steel and Composite Structures*, 3-5 September, Graz, Austria.
- [8] Hu G and Engelhardt M. Studies on the behavior of steel single-plate beam end connections in a fire. *Struct Eng Int* 2012, 22(4): 462-469.
- [9] Yu H, Burgess I, Davison J, and Plank R. Component Modelling of Flexible End-plate Connections in Fire. *Steel Structures* 2009, 9(1): 1-15.
- [10] Wang W, Li G, and Dong Y. Experimental study and spring-component modelling of extended end-plate joints in fire. *J Constr Steel Res* 2007, 63(8): 1127-1137.
- [11] Wang W, Li G, and Dong Y. A practical approach for fire resistance design of extended end-plate joints. *J Constr Steel Res* 2008, 64(12): 1456-1462.
- [12] Hu G and Engelhardt M. Experimental investigation of steel single plate beam end connections at elevated temperature. *Eng Struct* 2014, 58: 141-151.
- [13] Daryan A and Yahyai M. Modeling of bolted angle connections in fire. *Fire Saf J* 2009, 44(7): 976-988.
- [14] Kodur V, Naser M, Pakala P, and Varma A. Modeling the response of composite beam-slab assemblies exposed to fire. *J Constr Steel Res* 2013, 80: 163-173.
- [15] Selamat S and Garlock M. A comparison between the single plate and angle shear connection performance in fire. *ASCE structures congress. Las Vegas 2011, NV*: 416-426.

- [16] Selamat S and Garlock M. Predicting the maximum compressive beam axial force during fire considering local buckling. *J Constr Steel Res* 2012, 71: 189-201.
- [17] Selamat S and Garlock M. Fire resistance of steel shear connections. *Fire Saf J* 2014, 68: 52-60.
- [18] Hantouche E, Abboud N, Morovat M, and Engelhardt M. Analysis of steel bolted double angle connections subjected to fire temperatures. *J Constr Steel Res* (in review)
- [19] Dassault Systems, RI: Hibbitt, Karlsson, & Sorensen (2012). ABAQUS Version 6.12 User's Manual.
- [20] University of Sheffield (2008). EPSRC project EP/C510984/1: robustness of joints in fire. <<http://fireresearch.group.shef.ac.uk/downloads.html>>, (February, 2014).
- [21] American Institute of Steel Construction (AISC). Specification for structural steel buildings. ANSI/AISC 360-10, 2010, Chicago, IL.
- [22] Lee J, Morovat M, Hu G, Engelhardt M, and Taleff E. Experimental investigation of mechanical properties of ASTM A992 steel at elevated temperatures. *Eng J* 2013;50(4): 249-272.
- [23] American Institute of Steel Construction (AISC). Specification for structural steel buildings. ANSI/AISC 360-15, 2015, Chicago, IL.
- [24] European Committee for Standardization (CEN). (2005). Eurocode 3: Design of Steel Structures --- Part 1-8: Design of Joints and Building Frames. BS EN 1993-1-8, Brussels.
- [25] Li T, Nethercot D, and Choo B. Behaviour of Flush End-plate Composite Connections with Unbalanced Moment and Variable Shear/Moment Ratios II. Prediction of Moment Capacity. *J Constr Steel Res* 1996, 38(2): 165-198.
- [26] Usmani A, Rotter J, Lamont S, Sanad A, and Gillie M. Fundamental principles of structural behavior under thermal effects. *Fire Saf J* 2001, 36: 721–744.

